RNA:DNA hybrids in the human genome have distinctive nucleotide characteristics, chromatin composition, and transcriptional relationships.

Julie Nadel,[1] Rodoniki Athanasiadou,[1,a] Christophe Lemetre,[1,b] N. Ari Wijetunga,[1] Pilib Ó Broin,[1] Hanae Sato,[1] Zhengdong Zhang,[1] Jeffrey Jeddeloh,[2] Cristina Montagna,[1] Aaron Golden,[1] Cathal Seoighe,[3] John M. Greally[1]

[1]Department of Genetics, Albert Einstein College of Medicine, Bronx, NY 10461, USA

[2]Roche-NimbleGen, Madison, WI 53711, USA

[3]School of Mathematics, Statistics and Applied Mathematics, National University of Ireland Galway, Galway, Ireland

John M. Greally, Center for Epigenomics and Division of Computational Genetics, Department of Genetics, Albert Einstein College of Medicine, 1301 Morris Park Avenue, Bronx, NY 10461, USA. Email: john.greally@einstein.yu.edu

[a]Current address: New York University, Center for Genomics and Systems Biology, Department of Biology, 12 Waverly Place, New York, NY 10003, USA

[b]Current address: Integrated Genomics Operation, Memorial Sloan-Kettering Cancer Center, New York, NY 10065, USA.

Running title: **RNA:DNA hybrids in the human genome.**

ABSTRACT

RNA:DNA hybrids represent a non-canonical nucleic acid structure that has been associated with a range of human diseases and potential transcriptional regulatory functions. Mapping of RNA:DNA hybrids in human cells reveals them to have a number of characteristics that give insights into their functions. A directional sequencing approach shows the RNA component of the RNA:DNA hybrid to be purine-rich, indicating a thermodynamic contribution to their *in vivo* stability. The RNA:DNA hybrids are enriched at loci with decreased DNA methylation and increased DNase hypersensitivity, and within larger domains with characteristics of heterochromatin formation, indicating potential transcriptional regulatory properties. Mass spectrometry studies of chromatin at RNA:DNA hybrids shows the presence of the ILF2 and ILF3 transcription factors, supporting a model of certain transcription factors binding preferentially to the RNA:DNA conformation. Overall, there is little to indicate a dependence for RNA:DNA hybrids forming co-transcriptionally, with results from the ribosomal DNA repeat unit instead supporting a model of RNA generating these structures *in trans*. The results of the study indicate heterogeneous functions of these genomic elements and new insights into their formation and stability *in vivo*.

INTRODUCTION

The complex regulatory process leading to gene expression involves, as a major upstream influence, the effects of transcription factors (TFs) binding to specific DNA motifs. This TF binding recruits complexes that generate a favorable environment for transcription through chromatin organizational modifications, and ultimately leads to the local recruitment and activation of an RNA polymerase complex. The targeting of TFs to specific locations is an informational puzzle, as the number of potential binding sites represented by their generally short sequence binding motifs vastly exceeds the minority used *in vivo.* This observation suggests that there is additional information present in genomic organization that determines the selection of this subset of sequence motifs. Studies aiming to identify these extra layers of genomic information have revealed influences of chromatin organization (Natarajan et al. 2012; Neph et al. 2012; Wang et al. 2012; Yip et al. 2012) and DNA methylation (Yip et al. 2012; Hu et al. 2013; Medvedeva et al. 2014), each of which can facilitate or reduce TF binding to cognate motifs.

The role of the conformation of the DNA molecule *in vivo* is less well studied. While it is known that nucleic acids can form numerous non-canonical conformations (Schlick 2010), the influence of these conformations in living cells remains under-studied. There is, however, evidence from *in vitro* assays that DNA conformation influences binding of proteins (Zhou et al. 2015). As examples, the SP1 transcription factor binds preferentially to the intra-strand G-quadruplex structure *in vitro* (Raiber et al. 2012), while we have found the methyl-binding domain of the Mecp2 protein to bind preferentially to single-stranded DNA (ssDNA), also *in vitro* (Khrapunov et al. 2014).

Such observations indicate that the exploration of these and other non-canonical structures occurring *in vivo* may be fruitful in adding a layer of information to enhance the interpretability of transcriptional regulatory processes. The potential for ssDNA to occur in living cells, prompted

by the results of our Mecp2 studies (Khrapunov et al. 2014), raised the question about how such structures could be created and maintained stably *in vivo*. One candidate process to mediate the stable formation of ssDNA is the generation of an RNA:DNA hybrid on one DNA strand leaving the other strand in a single-stranded conformation, a nucleic acid structure referred to as an R-loop (Aguilera and Garcia-Muse 2012).

Formation of an R-loop has multiple potential consequences in terms of local organization of transcriptional regulatory elements. The helical conformation of the RNA:DNA hybrid differs from the B-form typical of double-stranded DNA (dsDNA), instead creating a conformation intermediate with the A-form associated with dsRNA (Roberts and Crothers 1992). A locus forming an RNA:DNA hybrid therefore creates a double-stranded A/B intermediate conformation, with a second target for single-stranded nucleic acid binding proteins on the complementary, displaced DNA strand. Another property of the R-loop is the displacement by the RNA of G-rich ssDNA (Roy et al. 2008; Roy and Lieber 2009), allowing the formation of intramolecular G-quadruplex structures (Murat and Balasubramanian 2014). The potential that RNA:DNA hybrids may be resistant to the activity of DNA methyltransferases has previously been proposed (Ginno et al. 2012), as has their failure to organize DNA into a nucleosomal conformation (Dunn and Griffith 1980), further adding to their local influence on nucleic acid organization.

Stable maintenance of an RNA:DNA hybrid is subject to many influences. As well as the suggestion that these structures are more likely to be generated in G-rich DNA (Roy et al. 2008; Roy and Lieber 2009), there is also evidence that they are found at loci where the DNA is nicked (Roy et al. 2010), in sequences with unusual GC skewing (Ginno et al. 2013) or with greater polypurine content in the RNA molecule (Ratmeyer et al. 1994), while the concurrent creation of G-quadruplexes may also help to stabilize the local structural conformation (Wanrooij et al. 2012). Transcription of a locus has been positively associated with RNA:DNA hybrid formation (Tracy and Lieber 2000; Loomis et al. 2014), presumably by the RNA acting *in cis* with

the DNA from which it was transcribed, but there is evidence in yeast that Rad51 can facilitate RNA molecules *in trans* also forming RNA:DNA hybrids (Wahba et al. 2013). Mutations of enzymes such as RNase H (Wahba et al. 2011), RNA helicases (Mischo et al. 2011) and topoisomerases (Tuduri et al. 2009) have been found to be associated with the increased formation of RNA:DNA hybrids, supporting a model in which these enzymes normally function to remove these structures from the genome. The presence of RNA:DNA hybrids at ribosomal DNA repeats appears to be a conserved feature from yeast (Chan et al. 2014) to human cells (Ginno et al. 2012), for which any associated physiological role remains unclear.

Functionally, RNA:DNA hybrids and their associated ssDNA regions have been found to have numerous properties *in vitro* and *in vivo* in a range of organisms. The immunoglobulin class switch locus has been found to form RNA:DNA hybrids in a transcription-dependent manner (Reaban and Griffin 1990; Daniels and Lieber 1995). In fission yeast, Nakama and colleagues performed histone RNA immunoprecipitation and identified an RNA:DNA hybrid encoded by a non-coding RNA (ncRNA) in centromeric heterochromatin, requiring intact RNA interference (RNAi) machinery for its formation (Nakama et al. 2012). RNA:DNA hybrids were found to be enriched in regions of condensed chromatin marked by histone H3 serine 10 (H3S10) phosphorylation in yeast, *C. elegans* and human HeLa cells (Castellano-Pozo et al. 2013). Repression on a more local scale was observed in *Arabidopsis thaliana,* in which the formation of an R-loop at a heterochromatic part of the *COOLAIR* promoter is stabilized by binding by the ssDNA-binding protein homeodomain protein AtNDX, leading to local transcriptional silencing effects (Sun et al. 2013). A study of RNA:DNA hybrids formed at CpG islands found these sites to be lacking DNA methylation (Ginno et al. 2012). RNA:DNA hybrids appear to be formed constitutively at telomeres in yeast by telomeric repeat containing RNA (TERRA) where they appear to be well tolerated (Pfeiffer et al. 2013). An R-loop consisting of an RNA:DNA hybrid and an associated G-quadruplex are found at the replication origin of mitochondrial DNA and

appear to have transcriptional termination properties (Wanrooij et al. 2012). The functions attributed to RNA:DNA hybrids are thus diverse and appear to have a major degree of dependence upon their genomic context.

RNA:DNA hybrids are being increasingly associated with human diseases, with a major concern that their presence predisposes a locus to chromosomal breakage. For example, it has been shown that R-loops are processed by the nucleotide excision repair endonucleases XPF and XPG into double strand breaks (Sollier et al. 2014), and both BRCA1 (Hatchi et al. 2015) and BRCA2 (Bhatia et al. 2014) have been implicated as major processing enzymes involved in the resolution of RNA:DNA hybrids. The potential contribution of RNA-mediated genome instability to neoplastic mutational events appears to warrant further investigation. The formation of RNA:DNA hybrids has also been associated with a number of neurological diseases. Senataxin (*SETX*) mutations are implicated in the dominant juvenile form of amyotrophic lateral sclerosis type 4 (ALS4) and a recessive form of ataxia oculomotor apraxia type 2 (AOA2) (Chen et al. 2004), while RNase H2 (*RNASEH2*) mutations are among those associated with Aicardi-Goutières syndrome, in which the accumulation of unusual nucleic acids triggers inflammatory and autoimmune responses (Gunther et al. 2015). SETX is an RNA/DNA helicase and RNase H specifically hydrolyzes the RNA in an RNA:DNA hybrid. Each enzyme has been associated with resolution of RNA:DNA hybrids *in vivo* (Skourti-Stathaki et al. 2011; Chon et al. 2013), prompting speculation that the formation of RNA:DNA hybrids is important in the mechanism of each associated disease. It should, however, be noted that in mice with *Setx* mutations the accumulation of RNA:DNA hybrids was limited to non-neurological tissues (Yeo et al. 2014), which would not support a mechanistic model requiring the formation of these structures in the cells presumably mediating the phenotype. Finally, it is known that triplet repeats are prone to forming unusual nucleic acid structures, including R-loops and RNA:DNA hybrids, a phenomenon conserved in organisms from prokaryotes (Lin et al. 2010) to mammalian cells

(Loomis et al. 2014). Trinucleotide repeat expansion diseases are therefore being evaluated for a potential contribution of nucleic acid structures to disease pathogenesis, with accumulating evidence that R-loops are involved in Fragile X syndrome (Colak et al. 2014; Groh et al. 2014; Loomis et al. 2014) and Friedreich's ataxia (Groh et al. 2014), with similar events also occurring in hexanucleotide repeat expansions (Haeusler et al. 2014). We refer the reader to a number of excellent recent reviews of this topic for more complete insights into these unusual nucleic acid structures and their disease associations (Aguilera and Garcia-Muse 2012; Groh and Gromak 2014; Skourti-Stathaki and Proudfoot 2014).

To establish a foundation for understanding their function, we mapped RNA:DNA hybrids genome-wide *in vivo* in two human cell lines with parallel transcriptional and proteomic studies. These studies provide new insights into how specific loci are preferentially selected as sites of formation of these structures, and allow the inference of some of their likely functional properties. These non-canonical nucleic acid structures occur in ribosomal DNA and at tens of thousands of loci in the remainder of the genome, with sequence characteristics indicating a polypurine-richness of the RNA in the hybrid that is likely to increase the thermodynamic stability of these structures. RNA:DNA hybrids appear to have heterogeneous and context-dependent properties, with subgroups showing relationships with local transcription and chromatin structural features, and a general trend towards decreased DNA methylation. On a more regional scale of hundreds of kilobases, RNA:DNA hybrids are enriched in regions of the genome with a greater abundance of L1 LINEs and CpG islands, and the chromatin modifications indicative of heterochromatin organization. These findings also support the possibility that the RNA generating these RNA:DNA hybrids is generated *in trans*, a set of results that combines to provide new insights into these non-canonical nucleic acid structures in human cells.

RESULTS

RNA:DNA immunoprecipitation (RDIP)

We optimized an assay previously published as DNA:RNA immunoprecipitation (DRIP) (Ginno et al. 2012) to map RNA:DNA hybrids, changing several components of the protocol. These updates include the pre-treatment of the cellular nucleic acid with RNase I, the use of sonication with the goal of minimizing bias in fragmenting the nucleic acid, and the addition of directional information about the strand derived from the RNA component of the hybrid. Given the extensive changes made, we distinguish the updated assay with the new acronym RDIP (RNA:DNA immunoprecipitation). The assay is based on the use of the S9.6 antibody, which is believed to recognize the intermediate A/B helical RNA:DNA duplex conformation, with little to no sequence specificity (Boguslawski et al. 1986). We performed extensive *in vitro* testing of the antibody to reconfirm these properties, including electrophoretic mobility shift assays and South-Western blots of oligonucleotides (including RNase H pre-treatment) that confirmed the necessary RNA:DNA hybrid specificity of the antibody (**Supplemental Figure S1a-e**).

The *in vivo* studies were focused on the primary, non-transformed, diploid IMR-90 lung fibroblast cell line because of the substantial genome-wide data available from the Roadmap Epigenomics Program (Chadwick 2012). For comparison, we isolated a clone of HEK 293T cells that we found to have the least copy number variability of several tested as determined by array comparative genomic hybridization (**Supplemental Figure S1f**). The immunoprecipitation using sonicated whole cell nucleic acid, pre-treated with RNase I, was optimized, and tested using a Southern dot blot using a $(TTAGGG)_n$ probe to confirm enrichment of the telomeric TERRA-associated R-loop (Pfeiffer et al. 2013) (**Supplemental Figure S1g**). This pre-treatment with RNase I was recently shown to be necessary to reduce noise due to the S9.6 antibody detecting RNA in unusual conformations (Zhang et al. 2015). To allow the immunoprecipitated RNA:DNA hybrid to be ligated into sequencing adapters, an approach

derived from RNA-seq library preparation was used. This provided the opportunity to introduce dUTP during second strand synthesis to reveal directional information about the strand on which the RNA molecule was located (Parkhomchuk et al. 2009). To confirm the RDIP-seq assay worked, we used peak calling analytical methodologies borrowed from ChIP-seq to identify the locations of RNA:DNA hybrids, followed by the use of single locus quantitative PCR to confirm enrichment in the immunoprecipitated material at these loci (**Supplemental Figure S1h**). Peaks were also verified at further loci using the orthogonal approach of bisulphite sequencing of non-denatured DNA to demonstrate the presence of the ssDNA that occurs at R-loops (Yu et al. 2003) (**Supplemental Figure S1i**).

Subcellular localization studies

The subcellular localization of RNA:DNA hybrids has been studied in multiple organisms using a number of techniques (Ginno et al. 2012; Wahba et al. 2013; Bhatia et al. 2014; Yeo et al. 2014) and was investigated in the current study using two separate approaches. The first used limited amplification of the HEK 293T RDIP-seq library with a PCR primer to which the Texas Red fluorophore had been conjugated. This was hybridized to control human metaphases for visualization. As early results suggested that the pericentromeric region of chromosome 9 was generating signal, a locus-specific probe targeting the subtelomeric region of the p arm of this specific chromosome was included in the fluorescence *in situ* hybridization (FISH) study. **Figure 1a** depicts the results of these studies. A strong signal at the centromere of chromosome 9 is observed, as well as from the p arms of the acrocentric chromosomes, indicating enrichment at the Nucleolar Organising Regions (NORs), where ribosomal DNA (rDNA) repetitive sequences are located.

The second subcellular localization approach employed was to use the S9.6 antibody for immunofluorescence of the HEK 293T cells. Consistent with previously published studies

(Ginno et al. 2012; Koo et al. 2015), a subnuclear enrichment within nucleoli (confirmed with an anti-fibrillarin antibody, **Figure 1b**) was observed. Of note was the additional cytoplasmic signal that has also been noted in prior studies (Koo et al. 2015). This signal may in part reflect signals from mitochondrial DNA (Brown et al. 2008) or the S9.6 antibody detecting ssRNA in unusual conformations (Zhang et al. 2015).

Ribosomal DNA studies

Prompted by the co-localization with the NORs seen in the subcellular localization studies, further investigation into RNA:DNA hybrid formation within ribosomal DNA was undertaken. The IMR-90 RDIP library was sequenced and mapped to a human reference genome including the consensus ribosomal DNA repeat unit (Gonzalez and Sylvester 1995) (accession number gi|555853|gb|U13369.1|HSU13369), following the same approach as Zentner and colleagues (Zentner et al. 2011). The results showed that ~2% of reads mapped to the ribosomal DNA repeat unit and the remainder to the sequenced majority of the human genome. The mapping of reads to the rDNA repeat unit is shown in **Figure 2**. The immunoprecipitated RNA:DNA hybrids map heterogeneously within this repeat unit, with accumulation of reads at the known exons of the rDNA gene, and others in the intergenic spacer (IGS) region.

To determine the relationship between the RNA:DNA hybrids and the transcribed sequences, RNA-seq on total RNA from the IMR-90 cells was performed without polyA selection or depletion of ribosomal RNA. This allowed deep sequencing of the expressed rRNA and co-localization with the RNA:DNA hybrid reads (**Figure 2**). The RDIP-seq reads in the 5' end of the repeat unit are precisely co-localized with the RNA-seq reads, but there is RNA:DNA hybrid formation with comparable read enrichment in the IGS region. Using K562 cell ChIP-seq data provided by Zentner and colleagues (Zentner et al. 2011), the RNA:DNA hybrids are found to be located upstream from the rDNA promoter and flanking the candidate *cis*-regulatory sequence in

the IGS region (**Figure 2**). The intergenic candidate *cis*-regulatory sequence was also shown to occur in embryonic stem cells, umbilical vein cells and normal human epidermal keratinocytes (Zentner et al. 2011), and thus appears to be constitutive. It is therefore reasonable to predict that the element is also present in the IMR-90 cells. Some of the rDNA RDIP-seq signal is attributable to RNA:DNA hybrid formation involving the canonical rRNA transcript, but further RNA:DNA hybrids are formed in the IGS ribosomal DNA region sparing the regions containing candidate *cis*-regulatory elements.

Genome-wide studies

Having defined the source of the rDNA signal, the focus turned to the majority of reads that mapped to the remainder of the sequenced genome. There are tens of thousands of RNA:DNA hybrid-forming loci (mapped as peaks using a ChIP-seq analytical approach) throughout the human genome (**Figure S2**), the same magnitude observed previously in DRIP-seq experiments (Ginno et al. 2012). There is a significant enrichment for loci shared by IMR-90 and HEK 293T cells, indicating that many RNA:DNA hybrid-forming loci may be constitutive across cell types. Focusing on the loci in the human diploid IMR-90 fibroblast cell line, RNA:DNA hybrids are demonstrated to be distributed genome-wide, with most of the peaks located in intergenic regions (**Figure 3a**). The enrichment of peaks in each of these major genomic contexts was calculated and the significance of enrichment was tested based on overlap (nucleotide occupancy) using permutation analyses. **Figure 3b** shows that promoters (and the highly correlated CpG island feature) are strongly enriched for RNA:DNA hybrids, and that they are distributed elsewhere in the genome at close to expected frequencies, apart from a modest but significant depletion at RefSeq gene bodies and intergenic regions (excluding promoter and lncRNA sequences).

As RNA:DNA hybrids in yeast have been shown to be enriched at transposons (Chan et al. 2014), their representation within sequences annotated as repetitive within the human genome was explored. In **Figure 3b,** the sequences annotated as low complexity and simple repeats by RepeatMasker are shown to be the most strongly over-represented, but satellite repeats are also found to be enriched in RNA:DNA hybrids. When the low complexity repeats were explored in greater detail, the strand on which the RNA component of the RNA:DNA hybrid was located was found to be composed of GA-rich, G-rich, and A-rich families of low complexity repeats. Additionally, within the satellite repeats that co-localized with the RNA of RNA:DNA hybrids, 76.5% of the repeats were $(GAATG)_n$ sequences.

It is known that purine-rich RNA binds *in vitro* with greater affinity to its pyrimidine-rich DNA complement than the equivalent purine-rich DNA sequence (Roberts and Crothers 1992; Ratmeyer et al. 1994), which may indicate a role for biochemical stability maintaining RNA:DNA hybrids *in vivo*. As the analyses of repetitive sequences suggested enrichment of purine-rich RNA in these RNA:DNA hybrids, this finding was explored more fully, testing for and finding from the genome-wide data a strong intramolecular skewing towards GA:CT enrichment (**Figure 4a**). To test globally whether this purine (GA) enrichment was present on the RNA-containing strand, the directional sequence information was used to examine nucleotide skewing on each strand at RNA:DNA hybrids, confirming the RNA-derived sequence to be strongly purine-enriched (**Figure 4b**). The 10% of peaks with the least tendency towards having the RNA enriched on one strand were removed from further analyses as being likely to over-represent experimental noise.

Relationship of RNA:DNA hybrids to local transcription

As some RNA:DNA hybrids have been found to have transcriptional termination properties (Belotserkovskii et al. 2010; Skourti-Stathaki et al. 2011), it was tested whether the RDIP

directional sequencing allowed the observation of the an orientation bias within genes. This tendency has been observed for transposable elements, which are believed to have different effects on gene function depending on their insertion orientation in gene bodies (Medstrand et al. 2002; Nellaker et al. 2012). The nucleotide skewing within each peak was visualized, revealing the purine-enriched component to be displaced 5' from the mid-point of the peak (**Figure S3**), which is consistent with the RDIP protocol using the RNA component of the RNA:DNA hybrid to prime second strand synthesis, proceeding unidirectionally 3' and relatively under-representing the region 5' to the RNA. This observation is independently supportive of the RNA component of the RNA:DNA hybrid being purine-enriched. There was a modest orientation bias against purine-rich sequences in the same orientation as the gene (**Figure S3b**), indicating that most but not all genes tolerate an RNA:DNA hybrid with the RNA on the transcribed strand.

To explore the relationship between RNA:DNA hybrid formation and transcription further, the proportions of genes with peaks were tested for transcription states from the RNA-seq data, finding that most transcribed RefSeq genes do not contain RNA:DNA hybrids but that the transcribed genes have a higher frequency of RNA:DNA hybrids than non-transcribed genes (7.75% compared with 6.09%, **Figure 5a**). The locations of these RNA:DNA hybrids within genes was defined using a metaplot, identifying the first ~1.5 kb downstream from the transcription start site (TSS) as the region most consistently enriched (**Figure 5b**). This region is also found to be modestly enriched in purine skewing for genes with and without RNA:DNA hybrids (**Figure 5c**). Surprisingly, given the transcriptional termination properties attributed to RNA:DNA hybrids (Belotserkovskii et al. 2010; Skourti-Stathaki et al. 2011), the transcriptional end site is notable for a slight depletion of these structures (**Figure 5b**). The information from lncRNAs also suggests a modest enrichment for RNA:DNA hybrids in the immediate vicinity of the TSS (**Figure S4**). The local generation of RNA:DNA hybrids has previously been described to be associated with transcription of the region (Roy and Lieber 2009; Loomis et al. 2014), so

the genes were stratified by expression level, finding that the proximal 1.5 kb region downstream from the TSS showed an increase in peaks associated with increasing quantiles of gene expression states (**Figure 5d**). The conclusion is that transcriptional levels have effects on the likelihood of forming RNA:DNA hybrids, and that local purine enrichment may increase the tendency of these structures to be formed in the ~1.5 kb immediately downstream of the TSS in a small subset of genes.

Relationship of RNA:DNA hybrids to regulators of transcription

To begin to infer any transcriptional regulatory function of the RNA:DNA hybrids from their genomic locations, studies were performed correlating RNA:DNA hybrid locations with enrichment or depletion for other chromatin and transcriptional regulators directly overlapping the RNA:DNA hybrids. Using IMR-90 bisulphite sequencing data from the Roadmap Epigenomics Project (accession number NA000020923.1), a modest decrease in DNA methylation within RNA:DNA hybrids was found compared with genome-wide levels, a finding which is consistent with the hypomethylation of DNA previously observed for RNA:DNA hybrids at CpG islands (Ginno et al. 2012) (**Figure S5a**). *In vitro* studies have shown RNA:DNA hybrids to be refractory to the formation of nucleosomal structures (Dunn and Griffith 1980), a finding supported by the observation that 7.46% of all RNA:DNA hybrids overlap DNase hypersensitive sites, representing a significant association genome-wide (**Figure S5b-c**). An analysis of these RNA:DNA hybrid-forming loci revealed an enriched polypurine $(GGAA)_n$ motif, which has been associated with binding by the FLI1 transcription factor (Mao et al. 1994) (**Figure S6a**).

A notable macro-scale organization of RNA:DNA hybrids was apparent in the human genome, with regions of dense and sparse RNA:DNA hybrid formation (example shown in **Figure S6b**). Using publicly-available ChIP-seq data from the IMR-90 cell line, it was possible to ask whether RNA:DNA hybrids in the human genome occur in regions of distinctive regulatory characteristics.

We have previously noted that there is extensive inter-correlation of genomic features (Fazzari and Greally 2004), making it difficult to discriminate specific associations when there are multiple correlating genomic variables. In order to explore the transcriptional and regulatory context of RNA:DNA hybrid peaks, regression models were fitted to the data, regularized using the least absolute shrinkage and selection operator (LASSO; (Tibshirani 1996)) with the peak density as the response variable. Least angle regression (LARS; (Efron et al. 2004)) was used, progressively adding covariates to the model and testing the significance of each added predictor using the covariance test statistic proposed by Lockhart *et al.* (Lockhart et al. 2014). The results of this procedure are shown in **Figure 6**. The first covariate to enter the model as significantly enriched in co-localization with RNA:DNA hybrids in 500 kb windows is the repressive histone mark, H3 lysine 27 trimethylation (H3K27me3), followed by CpG islands, L1 LINE retroelements and a further repressive histone mark, H3K9me3. The first eight covariates to enter the model all gave significant values of the covariance test statistic.

Local chromatin organizational studies using mass spectrometry

Finally, characterization of chromatin located at RNA:DNA hybrids was performed to identify the proteins enriched at these loci. Chromatin from HEK 293T cells was sonicated and a fraction immunoprecipitated with the S9.6 antibody, eluting the protein complexes using RNA:DNA hybrid oligonucleotides, and identifying local proteins through mass spectrometry (**Figure 7a**). These results and Western blotting validation of candidate proteins of interest are shown in **Figure 7b** and **Supplemental Table S2**. A number of different specific proteins plausibly associated with RNA:DNA hybrids were identified. RNA helicase A (encoded by *DHX9*) is a protein known to be involved in resolving RNA:DNA hybrids (Chakraborty and Grosse 2011) and is a necessary partner for FLI1 in tumourigenesis (Toretsky et al. 2006), while DNA binding protein B (YBX1) is known to bind to ssDNA (Stein et al. 2001) which should be part of R-loops

formed at these loci. ILF2 and ILF3 are also found in the chromatin at RNA:DNA hybrids. These are transcription factors known to recognize a purine-rich motif (Aoki et al. 1998), with our results raising the possibility that their binding may depend on the target nucleic acid existing in an RNA:DNA conformation.

The presence in local chromatin of RNA helicases and topoisomerases is consistent with prior reports that these enzymes are involved in the removal of RNA:DNA hybrids (Mischo et al. 2011; Groh et al. 2014). The question arose whether the IMR-90 and HEK 293T cells express the genes encoding the broader group of proteins implicated in removal of RNA:DNA hybrids *in vivo*. Using the RNA-seq data, nine of these genes were categorized into quartiles of expression, finding that all of the genes were expressed at high levels (**Figure S7**). The presence of the RNA:DNA hybrids in these cells is therefore in spite of robust levels of expression of genes encoding proteins that should actively remove them.

DISCUSSION

Mapping RNA:DNA hybrids in human cells has allowed new insights into the properties of these non-canonical nucleic acid structures. We confirm through subcellular localization studies prior observations that the ribosomal DNA harbors these structures (Ginno et al. 2012) (**Figure 1**). Additionally, we expand on findings in yeast (Chan et al. 2014) by mapping RNA:DNA hybrid locations within the human rDNA repeating unit, revealing these structures to be formed not only at the expressed rDNA gene but also in the intergenic spacer sequence (**Figure 2**). The signal from this repetitive sequence is necessarily composed of all rDNA repeat units in the genome, so we cannot distinguish events occurring within individual alleles, but we can make several inferences. Firstly, that the enrichment of RNA:DNA hybrids within the rDNA repeat unit is not uniform but is enriched at two types of loci, the exons of the rRNA genes and the intergenic spacer sequence where they spare present candidate *cis*-regulatory loci (**Figure 2**). The mapping of RNA:DNA hybrids to the rDNA gene exons is an interesting finding as it implies that the RNA associating with the rDNA is already spliced and not the primary transcript through the region. This is less supportive of a co-transcriptional model for RNA:DNA hybrid formation (Reaban and Griffin 1990; Daniels and Lieber 1995) and more indicative of rRNA acting *in trans* to generate these structures, as has been found for RNA:DNA hybrids in yeast (Wahba et al. 2013).

The mapping of reads to the rDNA repeat was consistent with the imaging data indicating the presence of RNA:DNA hybrids in nucleoli (**Figure 1**), allowing us to proceed with confidence to assess the distribution of the majority of the reads elsewhere in the genome. The first observation was that the RNA:DNA hybrids were not enriched in gene bodies relative to intergenic sequences (**Figure 3a-b**), again failing to support their presence being solely a function of recognized transcription. Furthermore, the rRNA model would suggest that spliced mRNAs might associate *in trans* with their genes of origin, but this is not reflected by over-

representation of RNA:DNA hybrids in RefSeq genes (**Figure 3b**). Instead we observe that a small proportion of genes have peaks within their bodies (**Figure 5a**), with a significantly higher proportion of expressed genes than silent genes containing RNA:DNA hybrids (**Figure 5d**). These tend to form in the ~1.5 kb immediately downstream of the transcription start site, where they are influenced by the level of transcription (**Figure 5d**) but can be found even in genes that are not measurably expressed by RNA-seq (**Figure 5a,d**), and are overall depleted in RefSeq gene bodies (**Figure 3b**). Transcription through a locus is therefore only modestly influential in generating these structures.

Adding to the tendency of the proximal 1.5 kb to form RNA:DNA hybrids is the enrichment at this location genome-wide for purine-skewed DNA in the transcriptional orientation of the gene (**Figure 5c**). We first noticed that purine enrichment may be a property of RNA:DNA hybrids *in vivo* when we found a strong enrichment for repetitive sequences composed of polypurines in our RepeatMasker analysis (**Figure 3b**). We confirm the purine skewing to be a general property of these sequences (**Figure 4** and **Figure S3**), which extends prior observations that suggested isolated G density (Roy and Lieber 2009) or GC (Ginno et al. 2013) skewing, to be characteristic of these loci. As purine-rich RNA binds to complementary pyrimidine-rich DNA with greater affinity than the same purine-rich DNA sequence *in vitro* (Roberts and Crothers 1992; Ratmeyer et al. 1994), this is likely to be a factor in the ability of the RNA to maintain displacement of the ssDNA in the R-loop structure.

While transcriptional termination has been described to be a property of RNA:DNA hybrids (Skourti-Stathaki et al. 2011) (reviewed in (Aguilera and Garcia-Muse 2012)), we observe that RNA:DNA hybrids are not enriched at the annotated ends of RefSeq genes and are, in fact, relatively depleted (**Figure 5b**). However, we see a small orientation bias in RefSeq genes, with a shift away from RNA:DNA hybrids with the RNA in the same orientation as transcription

(**Figure S3**). We interpret this to indicate that a subset of RNA:DNA hybrids may cause transcriptional disruption effects, but that it is not a universal property throughout the genome.

We can infer some likely functional properties of RNA:DNA hybrids by genomic co-localization and proteomic approaches. The genomic co-localization studies were both immediately at the RNA:DNA hybrid location and more broadly in their flanking regions, the latter prompted by what appeared to be higher-scale organization of the distribution of these loci (**Figure S6b**) and by prior studies in yeast (Nakama et al. 2012). The immediate local features included DNase hypersensitivity (**Figure S5b-c**), which is consistent with prior *in vitro* published findings that nucleosomes do not readily form on these structures (Dunn and Griffith 1980). The tendency of RNA:DNA hybrids to be resistant to acquisition of DNA methylation (Ginno et al. 2012) finds some support from our data, but the modest degree of relative hypomethylation indicates that the effects occur at only a small subset of loci. In the regional analysis of the co-localization of RNA:DNA hybrids and genomic sequence features within 500 kb windows of the genome, the enrichment found for CpG islands was not surprising given our observations that promoter-proximal sequences are enriched in RNA:DNA hybrids (**Figure 3b**). However, the enrichment in the same broader regions for the repressive H3K27me3 and H3K9me3 marks was unexpected for structures with the possibility of being co-transcriptionally generated. We interpret this to indicate one of the following three possibilities: that these regions are more transcribed than we can appreciate using the data available to us, allowing co-transcriptional formation of RNA:DNA hybrids, or that RNA forming RNA:DNA hybrids *in trans* is better able to target these regions, or that these structures are more stable in the context of repressive heterochromatin, with a causal model prompted by observations in fission yeast (Nakama et al. 2012) that would involve the RNA:DNA hybrids having a mechanistic role to induce the regional repressive organization.

The proteins revealed by the proteomic studies were consistent with the local presence of RNA:DNA hybrids and R-loops (**Figure 7**, **Supplemental Table S2**) , including RNA helicase

(DHX9) and single-stranded DNA binding properties. We were especially intrigued by the presence of the ILF2 and ILF3 components of the Nuclear Factor of Activated T-cells (NF-AT) transcription factor, which is required for T-cell expression of interleukin 2 and represents a target of the immunosuppressive Cyclosporin A and FK506 drugs (Kao et al. 1994). ILF2 (NF45) and ILF3 (NF90) are characterized by their binding to polypurine-rich interleukin gene enhancers (Aoki et al. 1998), and are described to have the property of being able to bind to dsRNA *in vitro* (Langland et al. 1999). This property, when combined with our finding of enrichment in chromatin at RNA:DNA hybrids, suggests that the selective binding of NF-AT at specific genomic locations may be dependent upon those sites being in an RNA:DNA hybrid conformation, which is structurally more similar to A-form dsRNA than B-form dsDNA (Roberts and Crothers 1992). The sequence motif $(GGAA)_n$ that we found to be enriched at RNA:DNA hybrids (**Figure S6a)** closely resembles that of the FLI1 transcription factor (Boeva et al. 2010). FLI1 is a master regulator of hematopoiesis (Pimkin et al. 2014) in the ETS family, and has been causally implicated in pediatric Ewing's sarcoma (Li et al. 2015). The oncogenic effect of FLI1 (as a fusion protein with EWS) is enhanced by RNA helicase A (Toretsky et al. 2006) which it appears to inhibit (Erkizan et al. 2015), an interaction that can in turn be inhibited by small molecules with therapeutic potential (Erkizan et al. 2009). Expression of EWS-FLI1 induces chromatin opening at sequences with the $(GGAA)_n$ motif (Riggi et al. 2014). The combination of the findings of binding to a polypurine-rich motif and interaction with RNA helicase A combine to suggest that FLI1 may also bind to an RNA:DNA nucleic acid conformation.

The model for RNA:DNA hybrid physiology that results from our studies indicates that they form as a result of an equilibrium between formation, stability and removal, with increased transcription having only a modest influence for the small subset we believe to be formed co-transcriptionally. Once formed, those at purine-skewed loci are likely to be more stable

thermodynamically, while the presence of enzymes like RNA helicase A in the local chromatin and the robust expression of genes encoding proteins that remove RNA:DNA hybrids (**Figure S7**) reflect how these structures remain despite active processes dedicated to their removal. The RNA:DNA hybrids form DNase hypersensitive structures which may facilitate or reflect binding of transcription factors with preferences for either the A/B form RNA:DNA duplex or the ssDNA in the R loop, and exist in large scale domains of repressed chromatin, with which their causal relationship is uncertain. We propose that the weight of evidence supports many of the RNA:DNA hybrids being formed *in trans*, by RNA transcripts originating from regions of the genome other than the location of the RNA:DNA hybrid itself. The ability of RNA to invade a double stranded DNA molecule *in trans* is being strikingly highlighted at present by CRISPR/Cas technology, which creates an RNA:DNA hybrid as part of an R-loop (Szczelkun et al. 2014). We find little evidence for the majority of the RNA:DNA hybrids *in vivo* to be located at recognizably transcribed sequences. More persuasively supporting a *trans* hypothesis is the finding that the RNA:DNA hybrids in the rDNA repeat unit map to processed rather than primary rRNA transcripts. The simplicity of the polypurine-skewed sequences at RNA:DNA hybrids potentially allows a limited number of transcripts to target a large number of loci. The nuclear-retained polypurine-rich RNAs found in mammalian cells represent a type of non-coding RNA of unclear function (Zheng et al. 2010) that could mediate such *trans* effects *in vivo*. Overall, it appears that there are numerous influences upon physiological RNA:DNA hybrid formation, the dissection of which will be essential if we are to understand the roles ascribed to them in disease states (Bacolla et al. 2001).

METHODS

S9.6 antibody production

The S9.6 antibody-producing hybridoma line was purchased from ATCC (HB08730), and the hybridoma line was grown in Integra Flasks by our institution's monoclonal antibody core facility in serum-free medium. The S9.6 antibody was then purified by the macromolecular therapeutics core facility using a Protein-G column and size exclusion. The antibody was validated using an electrophoretic mobility shift assay (EMSA) and southwestern blotting to test for specificity to RNA:DNA hybrid oligonucleotides. A full description of these experiments is provided in the **Supplemental Experimental Procedures**.

Immunofluorescence

HEK 293T cells were fixed in 4% paraformaldehyde for 10 minutes at room temperature, and then permeabilized for 10 min with 0.5% Triton-X-100. The cells were immunostained with anti-S9.6 antibody and anti-Fibrillarin antibody (Cell Signaling) for 1 hour, washed three times with phosphate buffered saline (PBS), and incubated with Alexa Fluor 488-labeled anti-mouse IgG antibody and Alexa Fluor 568 labeled anti-rabbit IgG antibody (Invitrogen) for 30 minutes at room temperature. Finally, cells were mounted in mounting solution ProLong Gold with DAPI (Invitrogen).

FISH

Fluorescence *in situ* hybridization (FISH) was performed using our previously published approach (Montagna et al. 2002). For the experiment described, 2 µg of DNA from the Illumina RDIP-seq library were labeled by nick translation using spectrum orange-dUTP (Invitrogen, Carlsbad, CA). A locus-specific BAC clone (9p TelVysion probe #05J03-009) mapping to

chromosome 9 was labeled in green using Spectrum Green (Vysis, Abbott Molecular, Des Plaines, IL). Both probes were hybridized to 46,XY control metaphases. The slides were denatured with 50% formaldehyde/2xSSC at 80°C for 1.5 minutes and then dehydrated with serial ethanol washing steps (ice cold 70, 90, and 100% for 3 minutes each). The probes were denaturated in the hybridization solution (50% dextran sulfate/2xSSC) at 85°C for 5 minutes, applied to the slides, and incubated overnight at 37°C in a humidified chamber. The slides were then washed 3 times for 5 minutes with 50% formamide/2X SSC, 1X SSC and 4xSSC/0.1%Tween. Slides were dehydrated with serial ethanol washing steps (see above) and mounted with ProLong Gold antifade reagent with DAPI (Invitrogen, Carlsbad, CA) for imaging. Image acquisition is described in **Supplemental Experimental Procedures**.

RNA:DNA hybrid immunoprecipitation (RDIP)

The cell culture conditions for IMR-90 and HEK 293T cells are described in the **Supplemental Experimental Procedures**. Whole cell nucleic acid was isolated from HEK 293T cells and IMR-90 cells through a modified salting out extraction protocol (Miller et al. 1988). Nucleic acid was sonicated to an average size of 400-600 bp using the Covaris sonicator. The fragmented nucleic acid was then treated with RNase I (Ambion AM2294) to remove any ssRNA from the sample, phenol/chloroform purified and re-suspended in EB buffer. Part of the nucleic acid sample was set aside as an untreated input sample for comparative sequencing. Three micrograms of nucleic acid sample was then incubated overnight with the S9.6 antibody, following which the RNA:DNA hybrids were enriched by immunomagnetic precipitation using Dynabeads (M-280 Sheep anti-mouse IgG). The sample was then extracted through phenol/chloroform purification, precipitated in the presence of glycogen and re-suspended in EB buffer. A complete detailed protocol is available in the **Supplemental Experimental Procedures**. Enrichment of predicted peaks in the RDIP product was validated using

quantitative PCR (Quanta PerfeCTa SYBR Green Fastmix). The primer sequences used are provided in **Table S3**.

Directional RDIP-seq

Using RDIP and input material, directional RDIP-seq libraries were prepared using elements of a directional RNA-seq protocol modified from a previously published approach (Parkhomchuk et al. 2009). Starting the library preparation at the second strand synthesis step, the RNA of the RNA:DNA hybrid was nicked using RNase H treatment to serve as a primer for the DNA polymerase. The second strand was formed while incorporating dUTP to allow for directional sequencing and the identification of the RNA strand of the RNA:DNA hybrid. Next, the ends of fragments were repaired, adenosine tails added, and Illumina Tru-Seq strand-specific adaptors ligated (adaptor sequences in **Supplemental Table S4**). UNG treatment was utilized to degrade the dUTP-containing RNA strand of the RNA:DNA hybrid, and barcoded PCR primers were used to amplify the library while maintaining directionality. The complete RDIP-seq protocol is available in the **Supplemental Experimental Procedures**.

Prior to sequencing, the libraries were analyzed for quality of preparation using an Agilent Bioanalyzer high-sensitivity chip. Libraries were multiplexed and combined for sequencing using Illumina HiSeq 2500 150 bp paired-end sequencing in our institutional Epigenomics Shared Facility. Fastq files were generated through the Illumina CASAVA pipeline (v1.8). Sequencing reads were then run through the Wasp System (WASP v3.1.5 rev. 6632) hosted pipeline for primary data processing, as follows. The reads were aligned to the hg19 reference genome using Bowtie (v0.12.7), using non-default parameters of --tryhard (increasing the number of attempts bowtie uses to find an alignment and number of backtracks), -I 50 (the minimum insert size in basepairs for valid paired-end alignments) and -X 650 (the maximum insert size for valid paired-end alignments). Alignments were generated in SAM format, which

were then transformed into BAM files using Samtools (version 0.1.8). The aligned sequences in BAM format had PCR duplicates removed, and peaks were called based on input and IP files using MACS v1.4.2 (Zhang et al. 2008). RDIP-seq peaks for IMR-90 cells and two datasets for HEK 293T cells were then analyzed using the program CHANCE for quality of immunoprecipitation (Diaz et al. 2012). Based on the results of CHANCE, we discarded one of the HEK 293T datasets and continued on with one set of peaks for each cell line. All peaks containing "N" nucleotides were discarded. Custom code and parameters for this analysis can be found on our GitHub resource in the file "Peak Calling." Motif analysis of RNA:DNA hybrid peaks is described in the **Supplemental Experimental Procedures**.

R-loop validation through non-denaturing bisulphite conversion

RDIP-seq peaks were validated through non-denaturing bisulphite conversion. Whole cell nucleic acid was isolated from HEK 293T cells through a modified salting out extraction protocol as outlined in the **Supplemental Experimental Procedures**. Nucleic acid was digested with EcoRV-HF. Non-denaturing bisulphite treatment was performed according to a previously published protocol (Yu et al. 2003). Regions of interest were amplified through PCR after denaturing or non-denaturing bisulphite treatment using primers to converted or unconverted DNA. The PCR product was purified, cloned using a TOPO-TA cloning kit (Life Technologies) and sequenced. The primer sequences used in non-denaturing bisulphite validation for this study are provided in **Table S5**.

Directional RDIP-seq strandedness analysis

Due to using directional sequencing through the incorporation of dUTP, we were able to determine the RNA-derived sequence of the RNA:DNA hybrids. To do this, we used the BAM

flag information describing our aligned sequences (http://broadinstitute.github.io/picard/). The second read in the pair, representing the sequence derived from the RNA strand following degradation using UNG of the dUTP-incorporated complementary strand, has the bit flag identifiers of 163 or 147, indicating that it maps to the top or bottom strand of the reference genome, respectively. By measuring the number of RNA reads aligned to the top or bottom reference strand for each peak, we could assign each RDIP-seq peak a "strandedness" value, with +1 being all RNA-derived reads aligned to the top strand and -1 all RNA-derived reads aligned to the bottom strand. We removed the small minority (10%) of peaks with intermediate values of strandedness to decrease what we presumed to be experimental noise in our data set. Custom code for this analysis can be found on our GitHub resource in the file "Determining RNA Strand and Minus10 files."

RNA-seq of HEK 293T cells and IMR-90 cells

RNA was isolated from HEK 293T and IMR-90 cells using TRIzol extraction. Four biological replicates from each cell line were DNase treated, and Ribo-Zero rRNA removal (Ribo-Zero, Epicentre) was utilized for three of the four RNA samples, leaving a non-Ribo-Zero depleted sample for rRNA expression analysis. RNA-seq libraries were prepared using a directional RNA-seq protocol modified from a prior published approach (Parkhomchuk et al. 2009) and detailed in the **Supplemental Experimental Procedures** Directional Whole Transcriptome Sequencing protocol. Prior to sequencing, the libraries were assessed for quality using an Agilent Bioanalyzer high-sensitivity chip. The samples were multiplexed and sequenced using 100 bp single-end read sequencing on the Illumina HiSeq 2500 in our institutional Epigenomics Shared Facility. The TruSeq adaptor sequences used in this assay are provided in **Supplemental Table S6**.

After sequencing, fastq file generation was completed using the Illumina CASAVA pipeline (v1.8). Post-sequencing analysis was performed using the WASP pipeline (v3.1.5 rev. 6632), involving read alignment using gsnap (2012-07-20), with htseq (v0.5.3p3) used to determine read quantitation. Biological replicates were normalized using DESeq (Bioconductor) and RefSeq gene identifiers were assigned using biomaRt. Only gene expression assigned a RefSeq identifier was used for further analysis. Custom code for this analysis can be found on our GitHub resource under the file "RNAseq Analysis."

Ribosomal DNA analysis

In order to align our RDIP-seq reads to the rDNA repeating unit, we used the alignment approach of Zentner and colleagues (Zentner et al. 2011). We added the rDNA repeating unit fasta file (gi|555853|gb|U13369.1|HSU13369) to the start of the hg19 chromosome 13, replacing the telomeric "N" nucleotides. Duplicate reads were removed from the IMR-90 RDIP-seq and input fastq files using a custom perl script provided by Zentner and colleagues (Zentner et al. 2011), and the remaining reads were aligned to the hg19+rDNA genome file using Bowtie. Wiggle tracks were then created using FSeq, and counts representative of the reads aligned to the rDNA portion of chromosome 13 were isolated. The RDIP-seq wiggle track values were normalized by subtracting the input values from the RDIP values. The same pipeline was used to align the IMR-90 RNA-seq samples that did not have prior Ribo-Zero depletion to the rDNA sequence. Processed histone mark datasets from K562 cells for rDNA were provided by Zentner and colleagues (Zentner et al. 2011), and averaged across 50 bp windows across the rDNA repeating unit. Custom code for this analysis can be found on our GitHub resource under the file "Figure 2 – rDNA figure with Zentner histone marks" and the custom perl script under "Zentner removeDupsFromFastQ Perl Script."

Regression models of RNA:DNA hybrid peak density

We used LASSO regularized linear regression to explore the relationship between the density of RNA:DNA hybrid peaks in 500 kb windows and genomic features associated with transcription and regulation. LASSO regression fits a linear model subject to a constraint on the sum of the regression coefficients (Tibshirani 1996). The LARS algorithm, implemented in the *LARS* R package, was applied to determine the Lasso path. This algorithm provides the optimal values of the regression coefficients as the constraint on the sum of the coefficients is progressively relaxed (Efron et al. 2004). Tight constraint on the sum of the coefficients enforces sparseness on the model with the number of covariates in the model increasing as this constraint is relaxed. The covariance test statistic (Lockhart et al. 2014), implemented in the *covTest* R package, was used to test the significance of each additional covariate when it enters the model.

Co-Immunoprecipitation of RNA:DNA Hybrid Binding Proteins (CoIP)

Native chromatin was isolated using a sucrose gradient from HEK 293T cells. Chromatin was incubated overnight with S9.6 antibody or a non-specific control antibody (β-actin, Sigma A5441), following which immunoprecipitation was performed on each sample using immunomagnetic precipitation (Dynabeads M-280 Sheep anti-mouse IgG). RNA:DNA hybrid-binding protein complexes were then eluted using RNA:DNA hybrid oligonucleotides, with DNA:DNA oligonucleotides as a control. The oligonucleotide sequences used in this assay are provided in **Supplemental Table S7**. The resulting enriched proteins were run on a 12% polyacrylamide gel, stained with GelCode Blue (Life Technologies 24594) and tested using Mass Spectrometry (MS). Proteins which were considered to bind specifically to RNA:DNA hybrids were defined as those only present in the S9.6 immunoprecipitated sample and eluted with the RNA:DNA oligonucleotides, removing any proteins also present in the control samples (those isolated with the β-actin antibody, and with the S9.6 antibody eluted with the DNA:DNA

oligonucleotides). This analysis was performed using Scaffold3 proteome software (Searle 2010). Peptide counts were assigned to each protein identified through mass spectrometry by measuring the quantity of the identified peptides by their spectra, and filtered by those peptides that also occurred in negative control experimental samples. Candidate proteins identified by mass spectrometry were then validated using Western blotting using the antibodies described in **Supplementary Table S8**.

Custom Code

Analysis of RDIP-seq, RNA-seq, and code for all figures are included and annotated at:

https://github.com/GreallyLab/Nadel-et-al.-2015

DATA ACCESS

The data generated are all available through the Gene Expression Omnibus, accession number GSE68953 (http://www.ncbi.nlm.nih.gov/geo/query/acc.cgi?acc=GSE68953).

Reviewer URL:

http://www.ncbi.nlm.nih.gov/geo/query/acc.cgi?token=snqdscyclxgproh&acc=GSE68953

ACKNOWLEDGEMENTS

The project was funded by NIH R21 GM101880 grant to JMG. Einstein core facilities involved were the Genome Imaging Core, the High-Performance Computing Core, the Epigenomics Shared Facility, the Proteomics Core Facility, the Monoclonal Antibody Core Facility and the Genomics Core Facility, with support from the Albert Einstein Cancer Center (P30CA013330) and the Center for Epigenomics. JN was supported by the Training Program in Cellular and Molecular Biology and Genetics, (NIH T32 GM007491) and NAW by the Medical Student Training Program (NIH T32 GM007288). We thank Drs. Gabe Zentner and Peter Scacheri at Case Western Reserve University for sharing code and data to allow us to perform the rDNA studies as comparably as possible with their prior work.

AUTHOR CONTRIBUTIONS

J.M.G. and J.J. designed the original project. J.M.G., R.A. and J.N. designed the original experiments and the analytical approaches. J.N. executed the experiments and analyzed results. J.M.G. and J.N. wrote the manuscript. C.L., N.A.W. and Z.Z. contributed to analysis. P.O. and A.G. performed the motif analysis. H.S. performed the immunofluorescence studies, and the group of C.M. performed the FISH studies. C.S. performed the LASSO analysis.

DISCLOSURE DECLARATION

The authors report no conflicts of interest.

FIGURE AND TABLE LEGENDS

Figure 1: Subcellular localization studies.

In panel (a) we show the results of hybridization of the fluorescently-labeled RDIP-seq library to a control male metaphase preparation. The RDIP-seq library is shown in red, a bacterial artificial chromosome (BAC) probe mapping to chromosome 9 in green, and DNA counterstained by DAPI in blue. We observe a specific strong signal from the RDIP-seq library mapping to the p arms of acrocentric chromosomes (HSA13-15 and HSA21-22), indicating enrichment at the nucleolar organizing regions (NORs) encoding ribosomal RNAs, and at the pericentromeric region of chromosome 9.

In panel (b) we show the results of immunofluorescence using the S9.6 antibody (green) with an antibody to fibrillarin (red), demonstrating co-localization with the intranuclear S9.6 antibody signal (merge) and therefore enrichment in nucleoli. Further signal from the nuclear periphery and the cytoplasm using S9.6 is also observed, which may represent detection by this antibody of RNA conformations rather than RNA:DNA hybrids specifically (Zhang et al. 2015).

Figure 2: Mapping of RNA:DNA hybrids within the ribosomal DNA repeat unit.

The upper panel shows the results of RDIP-seq (gray) and RNA-seq (red), with genomic annotations and results of ChIP-seq analysis in K562 cells (Zentner et al. 2011) plotted below. RDIP-seq and RNA-seq data are both represented using a smoothed plot showing the number of reads aligned to each basepair of the repeating unit, while the ChIP-seq data signal intensity represents the mean value of non-overlapping 50 bp windows. RDIP-seq values were normalized by subtracting the frequencies of aligned reads of the input sample in each window. We find that RNA:DNA hybrids co-localize with the rRNA transcripts, but that there are also RDIP-seq peaks of comparable magnitude in the intergenic spacer (IGS) where no

transcriptional activity is apparent from RNA-seq. The RNA:DNA hybrids in the IGS are upstream of the promoter region and flank the upstream candidate *cis*-regulatory sequence where there is H3K4 methylation and acetylation of H3K9 and H3K27.

Figure 3: Genomic distribution of RNA:DNA hybrids.

In panel (a) we show that the proportion of reads mapping to rDNA is 2%, and break down the remaining 98% by genomic context, showing the majority of RNA:DNA hybrids (called as peaks using ChIP-seq analytical approaches) to be located in intergenic regions. To understand these RNA:DNA hybrid distributions, we calculated observed/expected ratios based on nucleotide occupancy of genomic features, and performed permutation analyses testing for the likelihood of randomized intersection (b), the results of which are shown in **Supplemental Table S1**. We found depletion of RNA:DNA hybrids at RefSeq gene bodies, intergenic regions, and SINE and DNA transposable elements but significant enrichment at promoters and CpG islands, and a number of purine-rich repetitive sequences.

Figure 4: Nucleotide skewing analyses.

In panel (a) we plot the skewing within a strand of A compared to T (x axis) or G compared to C (y axis) in the RNA:DNA hybrid peaks genome-wide. We find that the peaks are strongly over-represented for purine (G+A) and pyrimidine (C+T) skewing. As our sequencing approach allowed us to identify the RNA and DNA-derived strands separately in the RNA:DNA hybrid, in (b) we proceeded to test whether there was a relationship between skewing (based on the number of G+A divided by the total number of nucleotides) and each type of nucleic acid-derived sequence, finding a clear enrichment for purine skewing on the RNA-derived strand.

Figure 5: Transcriptional relationships of RNA:DNA hybrids.

In (a) the proportion of RNA:DNA hybrid peaks in transcribed genes is shown to be higher than in non-transcribed genes, but that the majority of genes do not contain RNA:DNA hybrids. In (b) a metaplot of RNA:DNA hybrid peaks is shown, illustrating the number of peaks intersecting with 100 bp windows, with the RNA of the hybrid on the transcribed strand of the gene (red) or the opposite strand (blue). This revealed an enrichment of the RNA-derived sequence on the transcribed strand in the first ~1.5 kb downstream from the transcription start site (TSS). A depletion of RNA:DNA hybrids is found at the transcription end site (TES). In (c) we show that the region immediately downstream from the TSS is purine-skewed, represented by skewing values of 100 bp windows averaged for all genes, but that this is to the same degree in genes that form RNA:DNA hybrids (blue) as those genes that do not form these structures (red). In (d) a metaplot of RefSeq genes (left) shows that the transcription level of genes (as measured by RNA-seq) is positively associated with the number of RN:DNA hybrids intersecting with 100 bp windows immediately downstream of the TSS. This reflects only modest increases in the small proportions of genes forming peaks (right), though found to be a significant relationship using a proportions test.

Figure 6: Macro-scale genomic associations of RNA:DNA hybrids.

We used a least absolute shrinkage and selection operator (LASSO) adaptive regression approach to explore the association of genomic sequence features with RNA:DNA hybrid density in 500 kb windows. The figure shows the order in which covariates enter the model as the constraint on the sum of the regression coefficients (x-axis) is progressively relaxed from 0 to its maximum value (corresponding to the ordinary least squares regression vector).

Figure 7: Chromatin organizational studies at RNA:DNA hybrids using mass spectrometry.

In panel (a) we show the experimental approach used for these proteomic studies. In (b) the altered pattern of enriched proteins compared with the input sample is seen using gel electrophoresis, and the results of Western blots confirming the enrichment of specific candidate proteins identified by mass spectrometry (ILF2, ILF3, hnRNP C1/C2), with SP1 and SP3 as controls known to bind to G-skewed DNA motifs.

REFERENCES

Aguilera A, Garcia-Muse T. 2012. R loops: from transcription byproducts to threats to genome stability. *Mol Cell* **46**: 115-124.

Aoki Y, Zhao G, Qiu D, Shi L, Kao PN. 1998. CsA-sensitive purine-box transcriptional regulator in bronchial epithelial cells contains NF45, NF90, and Ku. *Am J Physiol* **275**: L1164-1172.

Bacolla A, Cooper DN, Vasquez KM. 2001. Non-B DNA Structure and Mutations Causing Human Genetic Disease. In *eLS*, doi:10.1002/9780470015902.a0022657. John Wiley & Sons, Ltd.

Belotserkovskii BP, Liu R, Tornaletti S, Krasilnikova MM, Mirkin SM, Hanawalt PC. 2010. Mechanisms and implications of transcription blockage by guanine-rich DNA sequences. *Proc Natl Acad Sci U S A* **107**: 12816-12821.

Bhatia V, Barroso SI, Garcia-Rubio ML, Tumini E, Herrera-Moyano E, Aguilera A. 2014. BRCA2 prevents R-loop accumulation and associates with TREX-2 mRNA export factor PCID2. *Nature* **511**: 362-365.

Boeva V, Surdez D, Guillon N, Tirode F, Fejes AP, Delattre O, Barillot E. 2010. De novo motif identification improves the accuracy of predicting transcription factor binding sites in ChIP-Seq data analysis. *Nucleic Acids Res* **38**: e126.

Boguslawski SJ, Smith DE, Michalak MA, Mickelson KE, Yehle CO, Patterson WL, Carrico RJ. 1986. Characterization of monoclonal antibody to DNA.RNA and its application to immunodetection of hybrids. *J Immunol Methods* **89**: 123-130.

Brown TA, Tkachuk AN, Clayton DA. 2008. Native R-loops persist throughout the mouse mitochondrial DNA genome. *J Biol Chem* **283**: 36743-36751.

Castellano-Pozo M, Santos-Pereira JM, Rondon AG, Barroso S, Andujar E, Perez-Alegre M, Garcia-Muse T, Aguilera A. 2013. R loops are linked to histone H3 S10 phosphorylation and chromatin condensation. *Mol Cell* **52**: 583-590.

Chadwick LH. 2012. The NIH Roadmap Epigenomics Program data resource. *Epigenomics* **4**: 317-324.

Chakraborty P, Grosse F. 2011. Human DHX9 helicase preferentially unwinds RNA-containing displacement loops (R-loops) and G-quadruplexes. *DNA Repair (Amst)* **10**: 654-665.

Chan YA, Aristizabal MJ, Lu PY, Luo Z, Hamza A, Kobor MS, Stirling PC, Hieter P. 2014. Genome-wide profiling of yeast DNA:RNA hybrid prone sites with DRIP-chip. *PLoS Genet* **10**: e1004288.

Chen YZ, Bennett CL, Huynh HM, Blair IP, Puls I, Irobi J, Dierick I, Abel A, Kennerson ML, Rabin BA et al. 2004. DNA/RNA helicase gene mutations in a form of juvenile amyotrophic lateral sclerosis (ALS4). *Am J Hum Genet* **74**: 1128-1135.

Chon H, Sparks JL, Rychlik M, Nowotny M, Burgers PM, Crouch RJ, Cerritelli SM. 2013. RNase H2 roles in genome integrity revealed by unlinking its activities. *Nucleic Acids Res* **41**: 3130-3143.

Colak D, Zaninovic N, Cohen MS, Rosenwaks Z, Yang WY, Gerhardt J, Disney MD, Jaffrey SR. 2014. Promoter-bound trinucleotide repeat mRNA drives epigenetic silencing in fragile X syndrome. *Science* **343**: 1002-1005.

Daniels GA, Lieber MR. 1995. RNA:DNA complex formation upon transcription of immunoglobulin switch regions: implications for the mechanism and regulation of class switch recombination. *Nucleic Acids Res* **23**: 5006-5011.

Diaz A, Nellore A, Song JS. 2012. CHANCE: comprehensive software for quality control and validation of ChIP-seq data. *Genome Biol* **13**: R98.

Dunn K, Griffith JD. 1980. The presence of RNA in a double helix inhibits its interaction with histone protein. *Nucleic Acids Res* **8**: 555-566.

Efron B, Hastie T, Johnstone I, Tibshirani R. 2004. Least angle regression. doi:10.1214/009053604000000067: 407-499.

Erkizan HV, Kong Y, Merchant M, Schlottmann S, Barber-Rotenberg JS, Yuan L, Abaan OD, Chou TH, Dakshanamurthy S, Brown ML et al. 2009. A small molecule blocking oncogenic protein EWS-FLI1 interaction with RNA helicase A inhibits growth of Ewing's sarcoma. *Nature medicine* **15**: 750-756.

Erkizan HV, Schneider JA, Sajwan K, Graham GT, Griffin B, Chasovskikh S, Youbi SE, Kallarakal A, Chruszcz M, Padmanabhan R et al. 2015. RNA helicase A activity is inhibited by oncogenic transcription factor EWS-FLI1. *Nucleic Acids Res* **43**: 1069-1080.

Fazzari MJ, Greally JM. 2004. Epigenomics: beyond CpG islands. *Nat Rev Genet* **5**: 446-455.

Ginno PA, Lim YW, Lott PL, Korf I, Chedin F. 2013. GC skew at the 5' and 3' ends of human genes links R-loop formation to epigenetic regulation and transcription termination. *Genome Res* **23**: 1590-1600.

Ginno PA, Lott PL, Christensen HC, Korf I, Chedin F. 2012. R-loop formation is a distinctive characteristic of unmethylated human CpG island promoters. *Mol Cell* **45**: 814-825.

Gonzalez IL, Sylvester JE. 1995. Complete sequence of the 43-kb human ribosomal DNA repeat: analysis of the intergenic spacer. *Genomics* **27**: 320-328.

Groh M, Gromak N. 2014. Out of balance: R-loops in human disease. *PLoS Genet* **10**: e1004630.

Groh M, Lufino MM, Wade-Martins R, Gromak N. 2014. R-loops associated with triplet repeat expansions promote gene silencing in Friedreich ataxia and fragile X syndrome. *PLoS Genet* **10**: e1004318.

Gunther C, Kind B, Reijns MA, Berndt N, Martinez-Bueno M, Wolf C, Tungler V, Chara O, Lee YA, Hubner N et al. 2015. Defective removal of ribonucleotides from DNA promotes systemic autoimmunity. *J Clin Invest* **125**: 413-424.

Haeusler AR, Donnelly CJ, Periz G, Simko EA, Shaw PG, Kim MS, Maragakis NJ, Troncoso JC, Pandey A, Sattler R et al. 2014. C9orf72 nucleotide repeat structures initiate molecular cascades of disease. *Nature* **507**: 195-200.

Hatchi E, Skourti-Stathaki K, Ventz S, Pinello L, Yen A, Kamieniarz-Gdula K, Dimitrov S, Pathania S, McKinney KM, Eaton ML et al. 2015. BRCA1 recruitment to transcriptional pause sites is required for R-loop-driven DNA damage repair. *Mol Cell* **57**: 636-647.

Hu S, Wan J, Su Y, Song Q, Zeng Y, Nguyen HN, Shin J, Cox E, Rho HS, Woodard C et al. 2013. DNA methylation presents distinct binding sites for human transcription factors. *eLife* **2**: e00726.

Kao PN, Chen L, Brock G, Ng J, Kenny J, Smith AJ, Corthesy B. 1994. Cloning and expression of cyclosporin A- and FK506-sensitive nuclear factor of activated T-cells: NF45 and NF90. *J Biol Chem* **269**: 20691-20699.

Khrapunov S, Warren C, Cheng H, Berko ER, Greally JM, Brenowitz M. 2014. Unusual characteristics of the DNA binding domain of epigenetic regulatory protein MeCP2 determine its binding specificity. *Biochemistry* **53**: 3379-3391.

Koo CX, Kobiyama K, Shen YJ, LeBert N, Ahmad S, Khatoo M, Aoshi T, Gasser S, Ishii KJ. 2015. RNA Polymerase III Regulates Cytosolic RNA:DNA Hybrids and Intracellular MicroRNA Expression. *J Biol Chem* **290**: 7463-7473.

Langland JO, Kao PN, Jacobs BL. 1999. Nuclear factor-90 of activated T-cells: A double-stranded RNA-binding protein and substrate for the double-stranded RNA-dependent protein kinase, PKR. *Biochemistry* **38**: 6361-6368.

Li Y, Luo H, Liu T, Zacksenhaus E, Ben-David Y. 2015. The ets transcription factor Fli-1 in development, cancer and disease. *Oncogene* **34**: 2022-2031.

Lin Y, Dent SY, Wilson JH, Wells RD, Napierala M. 2010. R loops stimulate genetic instability of CTG.CAG repeats. *Proc Natl Acad Sci U S A* **107**: 692-697.

Lockhart R, Taylor J, Tibshirani RJ, Tibshirani R. 2014. A significance test for the lasso. doi:10.1214/13-AOS1175: 413-468.

Loomis EW, Sanz LA, Chedin F, Hagerman PJ. 2014. Transcription-associated R-loop formation across the human FMR1 CGG-repeat region. *PLoS Genet* **10**: e1004294.

Mao X, Miesfeldt S, Yang H, Leiden JM, Thompson CB. 1994. The FLI-1 and chimeric EWS-FLI-1 oncoproteins display similar DNA binding specificities. *J Biol Chem* **269**: 18216-18222.

Medstrand P, van de Lagemaat LN, Mager DL. 2002. Retroelement distributions in the human genome: variations associated with age and proximity to genes. *Genome Res* **12**: 1483-1495.

Medvedeva YA, Khamis AM, Kulakovskiy IV, Ba-Alawi W, Bhuyan MS, Kawaji H, Lassmann T, Harbers M, Forrest AR, Bajic VB et al. 2014. Effects of cytosine methylation on transcription factor binding sites. *BMC genomics* **15**: 119.

Miller SA, Dykes DD, Polesky HF. 1988. A simple salting out procedure for extracting DNA from human nucleated cells. *Nucleic Acids Res* **16**: 1215.

Mischo HE, Gomez-Gonzalez B, Grzechnik P, Rondon AG, Wei W, Steinmetz L, Aguilera A, Proudfoot NJ. 2011. Yeast Sen1 helicase protects the genome from transcription-associated instability. *Mol Cell* **41**: 21-32.

Montagna C, Andrechek ER, Padilla-Nash H, Muller WJ, Ried T. 2002. Centrosome abnormalities, recurring deletions of chromosome 4, and genomic amplification of HER2/neu define mouse mammary gland adenocarcinomas induced by mutant HER2/neu. *Oncogene* **21**: 890-898.

Murat P, Balasubramanian S. 2014. Existence and consequences of G-quadruplex structures in DNA. *Current opinion in genetics & development* **25**: 22-29.

Nakama M, Kawakami K, Kajitani T, Urano T, Murakami Y. 2012. DNA-RNA hybrid formation mediates RNAi-directed heterochromatin formation. *Genes Cells* **17**: 218-233.

Natarajan A, Yardimci GG, Sheffield NC, Crawford GE, Ohler U. 2012. Predicting cell-type-specific gene expression from regions of open chromatin. *Genome Res* **22**: 1711-1722.

Nellaker C, Keane TM, Yalcin B, Wong K, Agam A, Belgard TG, Flint J, Adams DJ, Frankel WN, Ponting CP. 2012. The genomic landscape shaped by selection on transposable elements across 18 mouse strains. *Genome Biol* **13**: R45.

Neph S, Vierstra J, Stergachis AB, Reynolds AP, Haugen E, Vernot B, Thurman RE, John S, Sandstrom R, Johnson AK et al. 2012. An expansive human regulatory lexicon encoded in transcription factor footprints. *Nature* **489**: 83-90.

Parkhomchuk D, Borodina T, Amstislavskiy V, Banaru M, Hallen L, Krobitsch S, Lehrach H, Soldatov A. 2009. Transcriptome analysis by strand-specific sequencing of complementary DNA. *Nucleic Acids Res* **37**: e123.

Pfeiffer V, Crittin J, Grolimund L, Lingner J. 2013. The THO complex component Thp2 counteracts telomeric R-loops and telomere shortening. *EMBO J* **32**: 2861-2871.

Pimkin M, Kossenkov AV, Mishra T, Morrissey CS, Wu W, Keller CA, Blobel GA, Lee D, Beer MA, Hardison RC et al. 2014. Divergent functions of hematopoietic transcription factors in lineage priming and differentiation during erythro-megakaryopoiesis. *Genome Res* **24**: 1932-1944.

Raiber EA, Kranaster R, Lam E, Nikan M, Balasubramanian S. 2012. A non-canonical DNA structure is a binding motif for the transcription factor SP1 in vitro. *Nucleic Acids Res* **40**: 1499-1508.

Ratmeyer L, Vinayak R, Zhong YY, Zon G, Wilson WD. 1994. Sequence specific thermodynamic and structural properties for DNA.RNA duplexes. *Biochemistry* **33**: 5298-5304.

Reaban ME, Griffin JA. 1990. Induction of RNA-stabilized DNA conformers by transcription of an immunoglobulin switch region. *Nature* **348**: 342-344.

Riggi N, Knoechel B, Gillespie SM, Rheinbay E, Boulay G, Suva ML, Rossetti NE, Boonseng WE, Oksuz O, Cook EB et al. 2014. EWS-FLI1 utilizes divergent chromatin remodeling mechanisms to directly activate or repress enhancer elements in Ewing sarcoma. *Cancer cell* **26**: 668-681.

Roberts RW, Crothers DM. 1992. Stability and properties of double and triple helices: dramatic effects of RNA or DNA backbone composition. *Science* **258**: 1463-1466.

Roy D, Lieber MR. 2009. G clustering is important for the initiation of transcription-induced R-loops in vitro, whereas high G density without clustering is sufficient thereafter. *Mol Cell Biol* **29**: 3124-3133.

Roy D, Yu K, Lieber MR. 2008. Mechanism of R-loop formation at immunoglobulin class switch sequences. *Mol Cell Biol* **28**: 50-60.

Roy D, Zhang Z, Lu Z, Hsieh CL, Lieber MR. 2010. Competition between the RNA transcript and the nontemplate DNA strand during R-loop formation in vitro: a nick can serve as a strong R-loop initiation site. *Mol Cell Biol* **30**: 146-159.

Schlick T. 2010. Topics in Nucleic Acids Structure: Noncanonical Helices and RNA Structure. In *Molecular Modeling and Simulation: An Interdisciplinary Guide*, Vol 21, pp. 205-236. Springer New York.

Searle BC. 2010. Scaffold: a bioinformatic tool for validating MS/MS-based proteomic studies. *Proteomics* **10**: 1265-1269.

Skourti-Stathaki K, Proudfoot NJ. 2014. A double-edged sword: R loops as threats to genome integrity and powerful regulators of gene expression. *Genes Dev* **28**: 1384-1396.

Skourti-Stathaki K, Proudfoot NJ, Gromak N. 2011. Human senataxin resolves RNA/DNA hybrids formed at transcriptional pause sites to promote Xrn2-dependent termination. *Mol Cell* **42**: 794-805.

Sollier J, Stork CT, Garcia-Rubio ML, Paulsen RD, Aguilera A, Cimprich KA. 2014. Transcription-coupled nucleotide excision repair factors promote R-loop-induced genome instability. *Mol Cell* **56**: 777-785.

Stein U, Jurchott K, Walther W, Bergmann S, Schlag PM, Royer HD. 2001. Hyperthermia-induced nuclear translocation of transcription factor YB-1 leads to enhanced expression of multidrug resistance-related ABC transporters. *J Biol Chem* **276**: 28562-28569.

Sun Q, Csorba T, Skourti-Stathaki K, Proudfoot NJ, Dean C. 2013. R-loop stabilization represses antisense transcription at the Arabidopsis FLC locus. *Science* **340**: 619-621.

Szczelkun MD, Tikhomirova MS, Sinkunas T, Gasiunas G, Karvelis T, Pschera P, Siksnys V, Seidel R. 2014. Direct observation of R-loop formation by single RNA-guided Cas9 and Cascade effector complexes. *Proc Natl Acad Sci U S A* **111**: 9798-9803.

Tibshirani R. 1996. Regression Shrinkage and Selection via the Lasso. *Journal of the Royal Statistical Society (Series B)* **58**: 267-288.

Toretsky JA, Erkizan V, Levenson A, Abaan OD, Parvin JD, Cripe TP, Rice AM, Lee SB, Uren A. 2006. Oncoprotein EWS-FLI1 activity is enhanced by RNA helicase A. *Cancer Res* **66**: 5574-5581.

Tracy RB, Lieber MR. 2000. Transcription-dependent R-loop formation at mammalian class switch sequences. *EMBO J* **19**: 1055-1067.

Tuduri S, Crabbe L, Conti C, Tourriere H, Holtgreve-Grez H, Jauch A, Pantesco V, De Vos J, Thomas A, Theillet C et al. 2009. Topoisomerase I suppresses genomic instability by preventing interference between replication and transcription. *Nat Cell Biol* **11**: 1315-1324.

Wahba L, Amon JD, Koshland D, Vuica-Ross M. 2011. RNase H and multiple RNA biogenesis factors cooperate to prevent RNA:DNA hybrids from generating genome instability. *Mol Cell* **44**: 978-988.

Wahba L, Gore SK, Koshland D. 2013. The homologous recombination machinery modulates the formation of RNA-DNA hybrids and associated chromosome instability. *eLife* **2**: e00505.

Wang J, Zhuang J, Iyer S, Lin X, Whitfield TW, Greven MC, Pierce BG, Dong X, Kundaje A, Cheng Y et al. 2012. Sequence features and chromatin structure around the genomic regions bound by 119 human transcription factors. *Genome Res* **22**: 1798-1812.

Wanrooij PH, Uhler JP, Shi Y, Westerlund F, Falkenberg M, Gustafsson CM. 2012. A hybrid G-quadruplex structure formed between RNA and DNA explains the extraordinary stability of the mitochondrial R-loop. *Nucleic Acids Res* **40**: 10334-10344.

Yeo AJ, Becherel OJ, Luff JE, Cullen JK, Wongsurawat T, Jenjaroenpoon P, Kuznetsov VA, McKinnon PJ, Lavin MF. 2014. R-loops in proliferating cells but not in the brain: implications for AOA2 and other autosomal recessive ataxias. *PLoS One* **9**: e90219.

Yip KY, Cheng C, Bhardwaj N, Brown JB, Leng J, Kundaje A, Rozowsky J, Birney E, Bickel P, Snyder M et al. 2012. Classification of human genomic regions based on experimentally determined binding sites of more than 100 transcription-related factors. *Genome Biol* **13**: R48.

Yu K, Chedin F, Hsieh CL, Wilson TE, Lieber MR. 2003. R-loops at immunoglobulin class switch regions in the chromosomes of stimulated B cells. *Nature immunology* **4**: 442-451.

Zentner GE, Tesar PJ, Scacheri PC. 2011. Epigenetic signatures distinguish multiple classes of enhancers with distinct cellular functions. *Genome Res* **21**: 1273-1283.

Zhang Y, Liu T, Meyer CA, Eeckhoute J, Johnson DS, Bernstein BE, Nusbaum C, Myers RM, Brown M, Li W et al. 2008. Model-based analysis of ChIP-Seq (MACS). *Genome Biol* **9**: R137.

Zhang ZZ, Pannunzio NR, Hsieh CL, Yu K, Lieber MR. 2015. Complexities due to single-stranded RNA during antibody detection of genomic rna:dna hybrids. *BMC Res Notes* **8**: 127.

Zheng R, Shen Z, Tripathi V, Xuan Z, Freier SM, Bennett CF, Prasanth SG, Prasanth KV. 2010. Polypurine-repeat-containing RNAs: a novel class of long non-coding RNA in mammalian cells. *J Cell Sci* **123**: 3734-3744.

Zhou T, Shen N, Yang L, Abe N, Horton J, Mann RS, Bussemaker HJ, Gordan R, Rohs R. 2015. Quantitative modeling of transcription factor binding specificities using DNA shape. *Proc Natl Acad Sci U S A* **112**: 4654-4659.

a

FISH

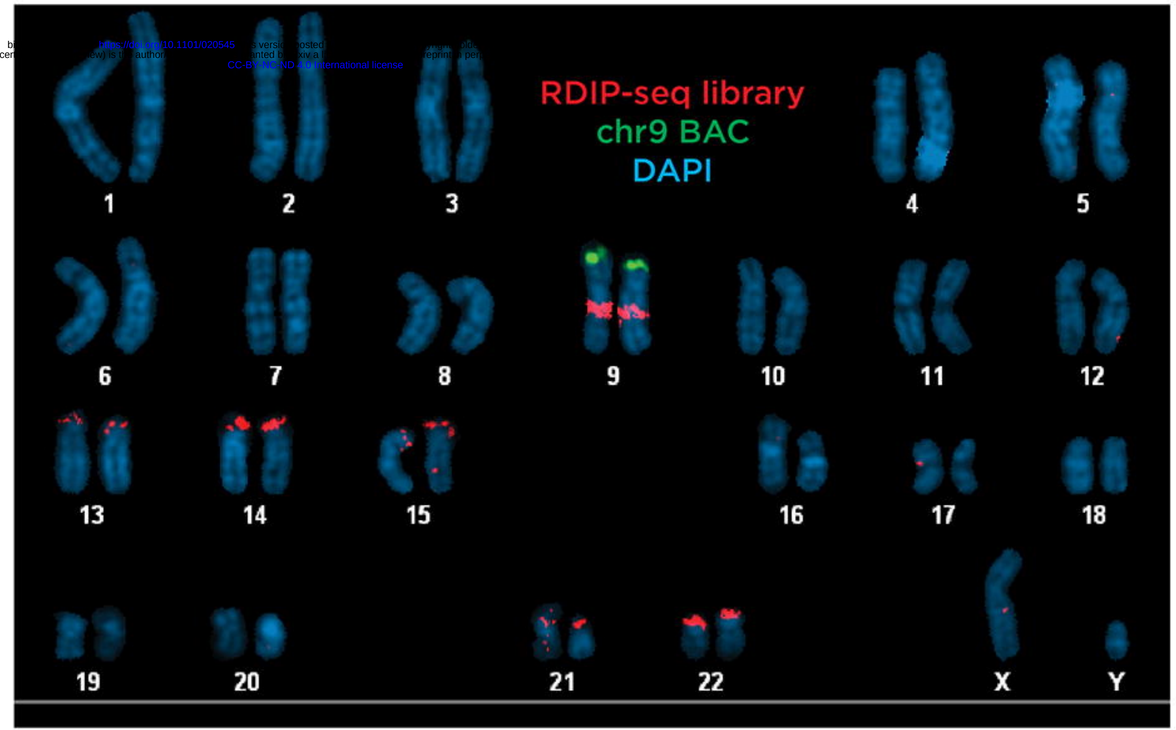

b

Immunofluorescence

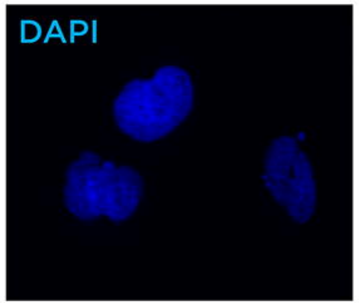

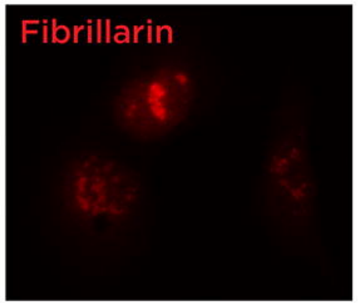

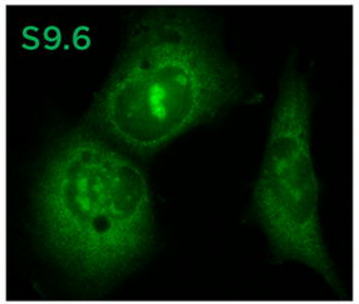

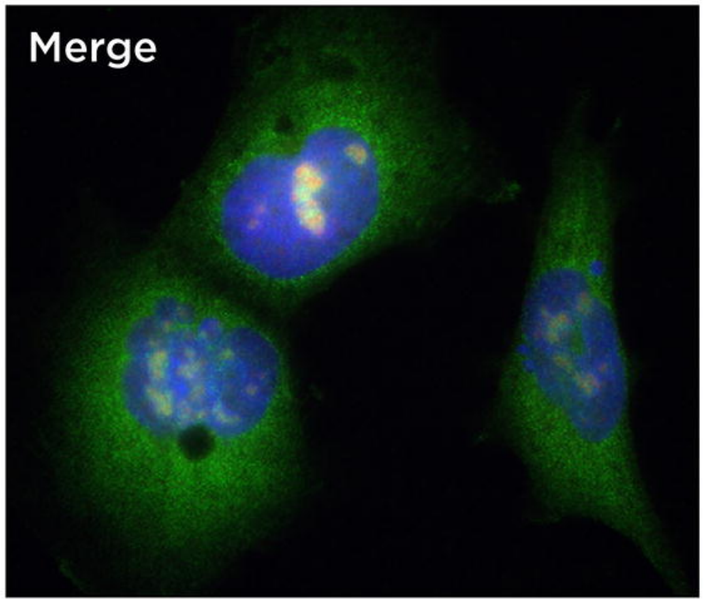

Nucleotide location within rDNA repeat unit

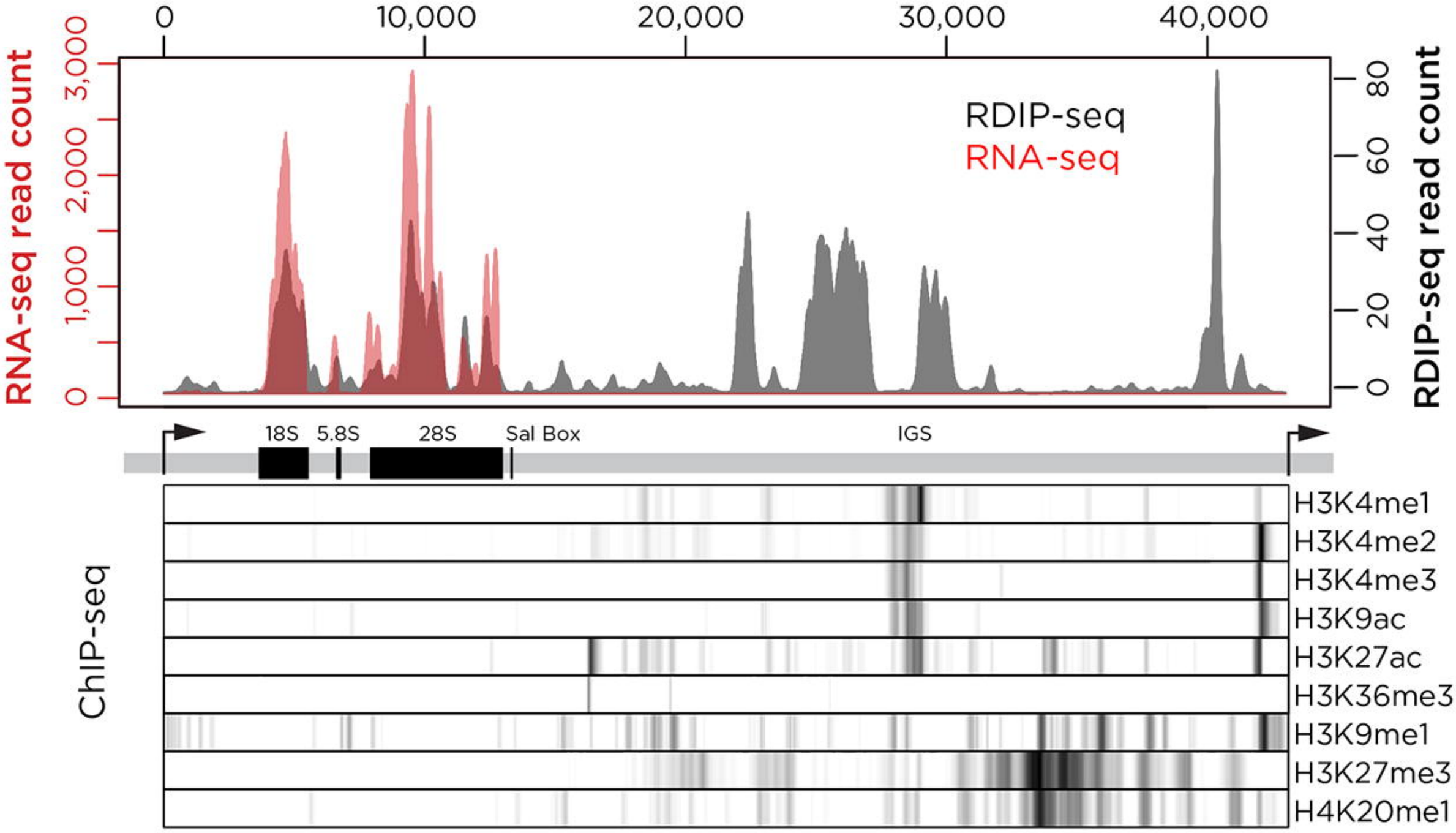

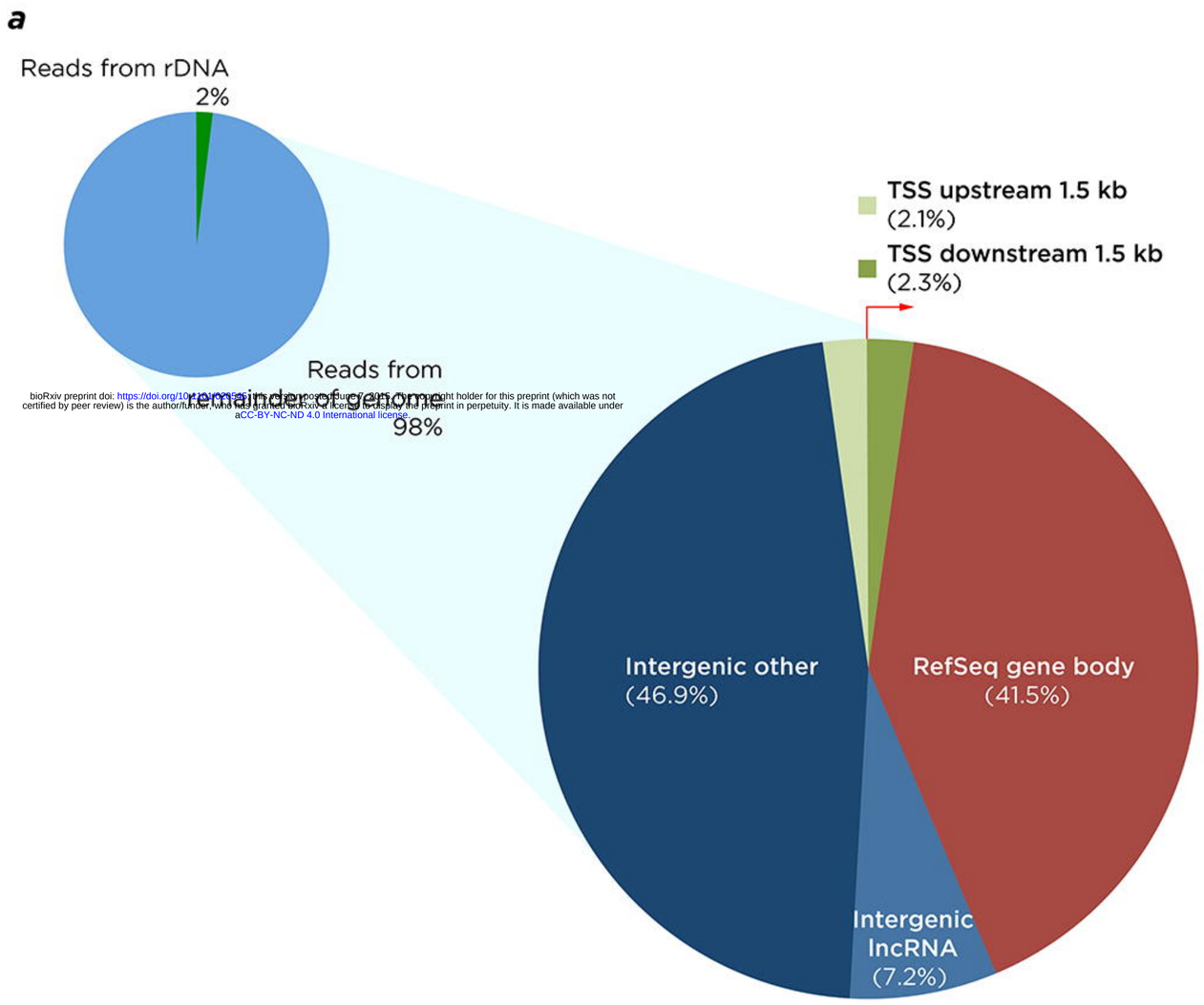

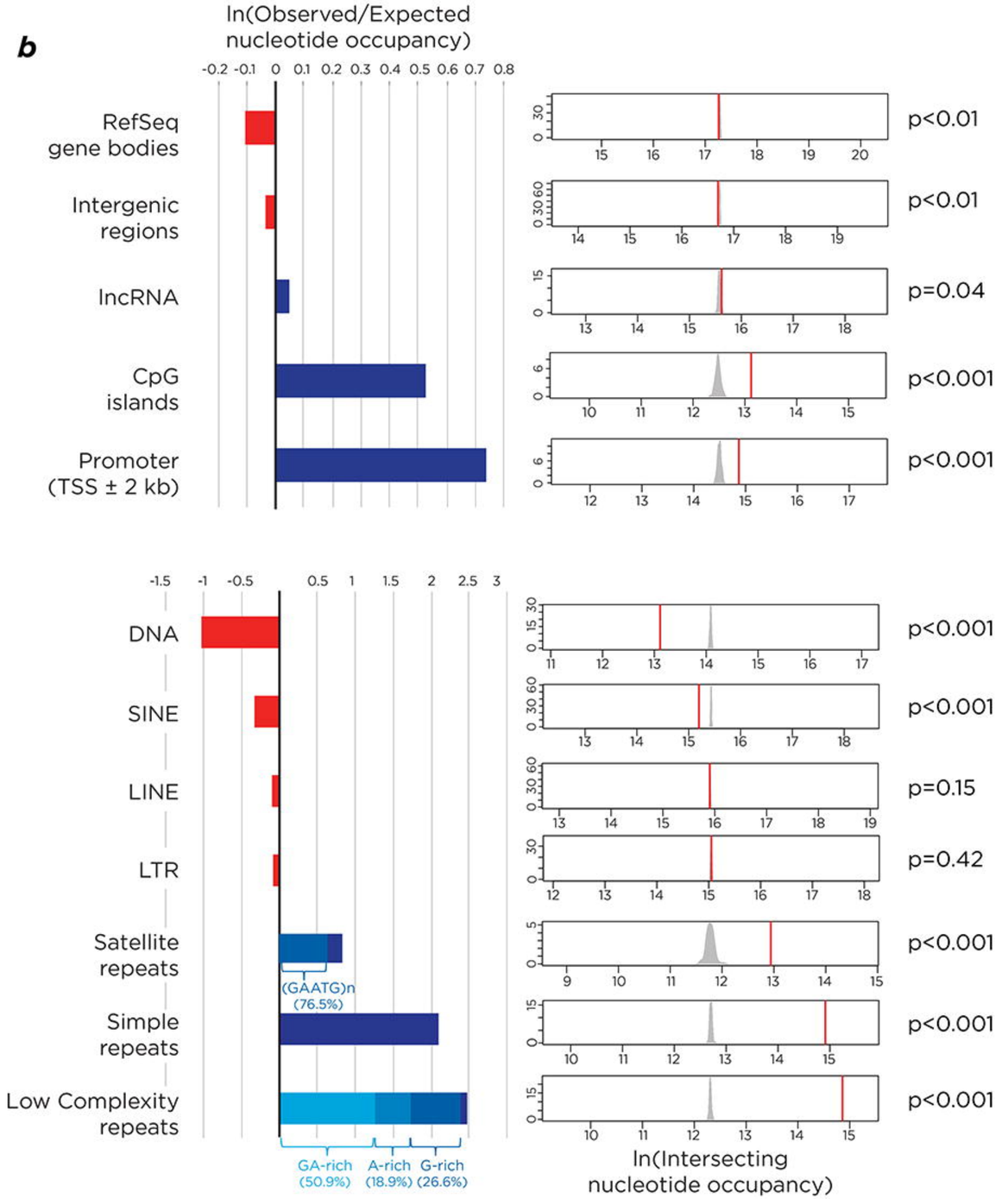

a

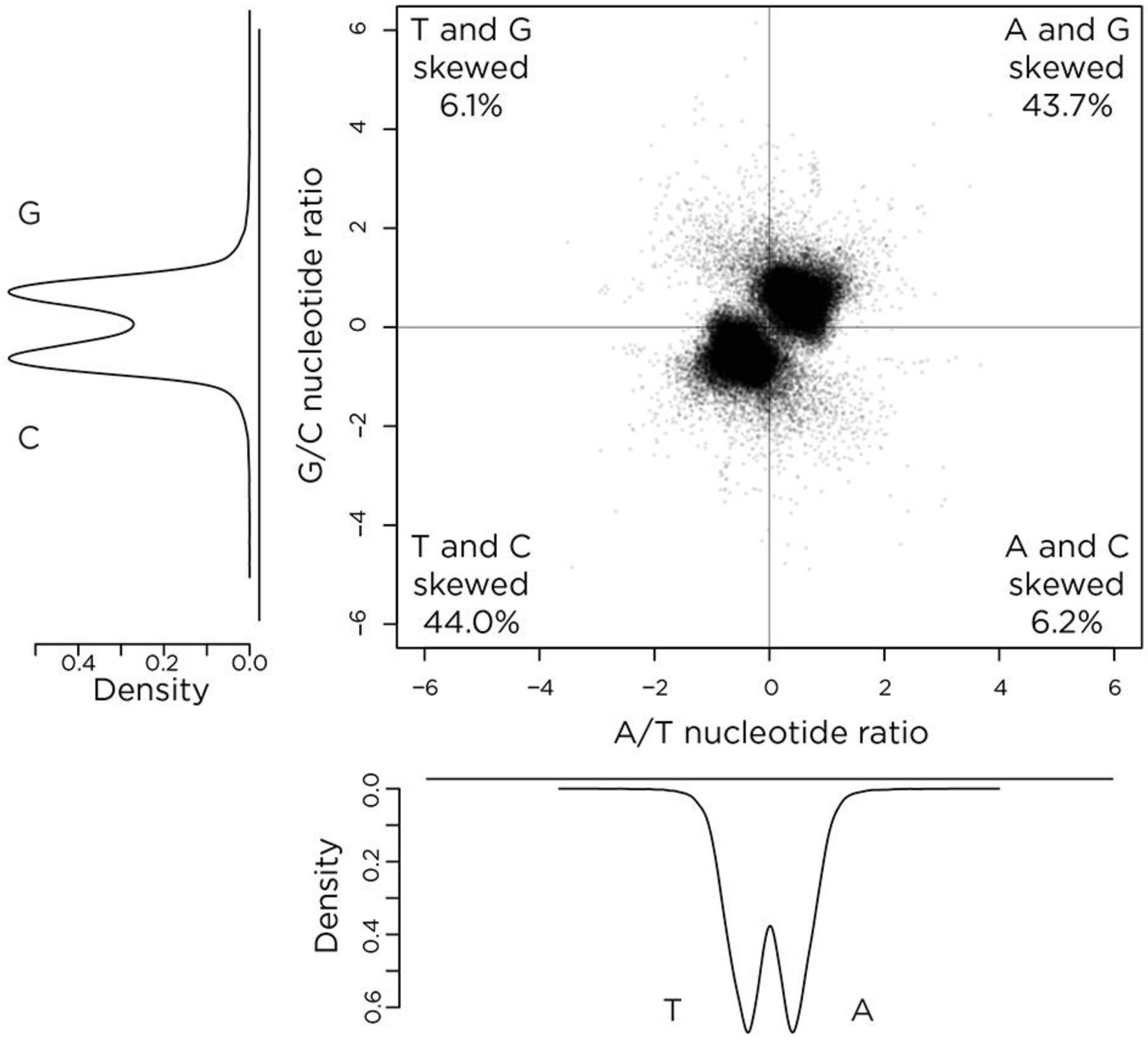

b

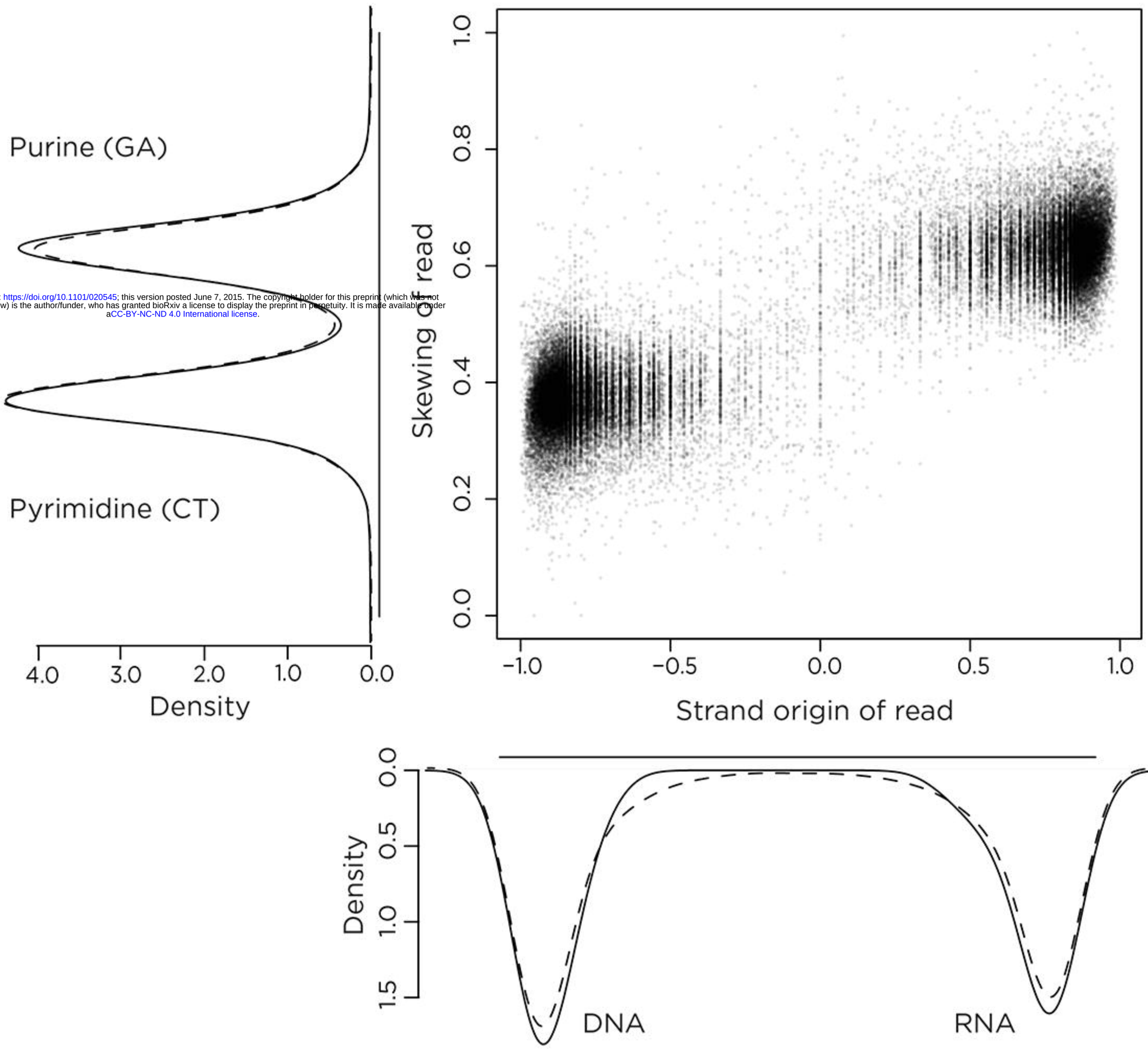

a

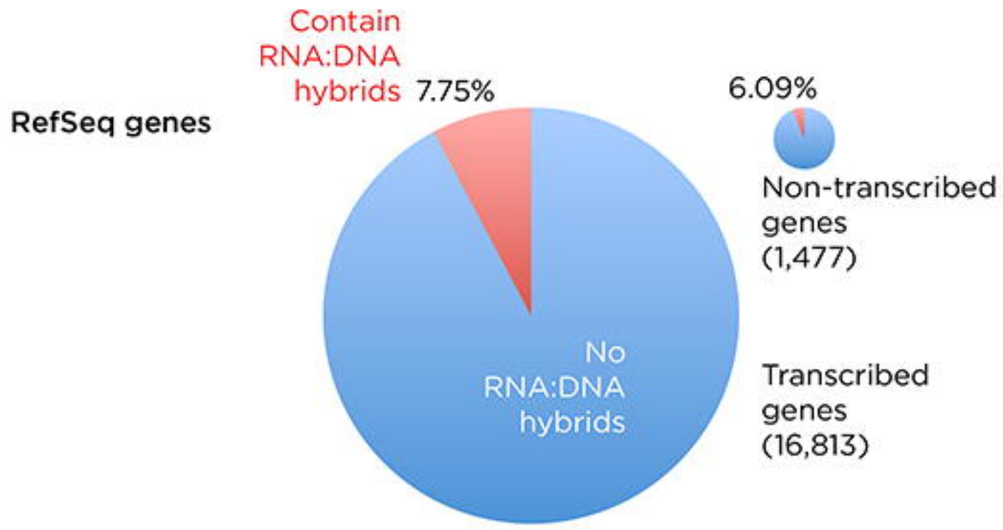

b

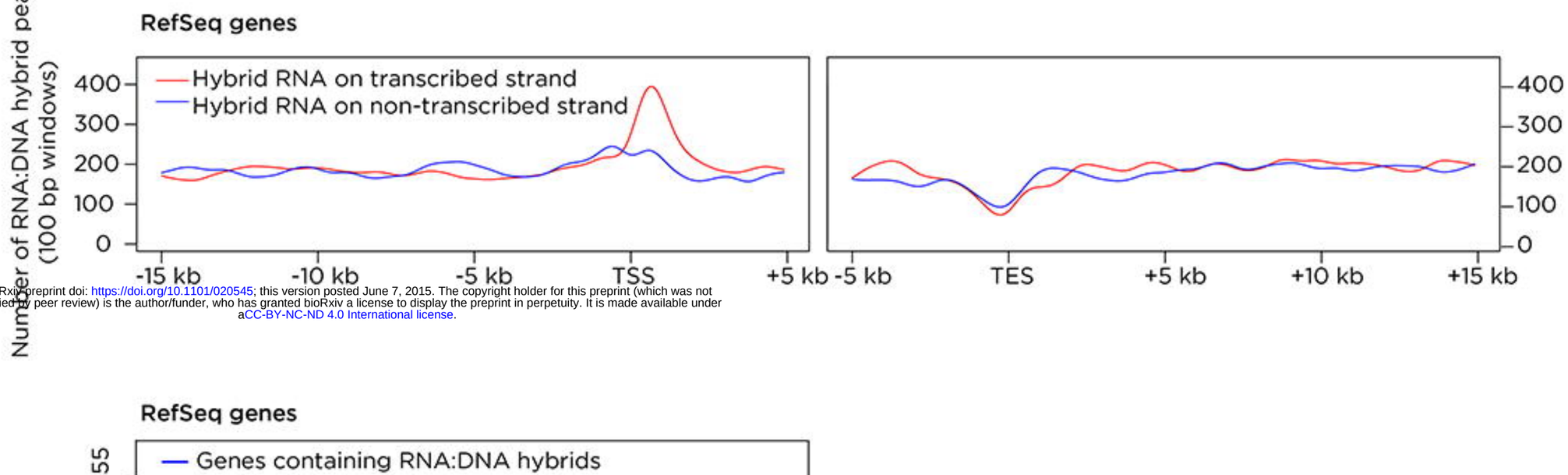

c

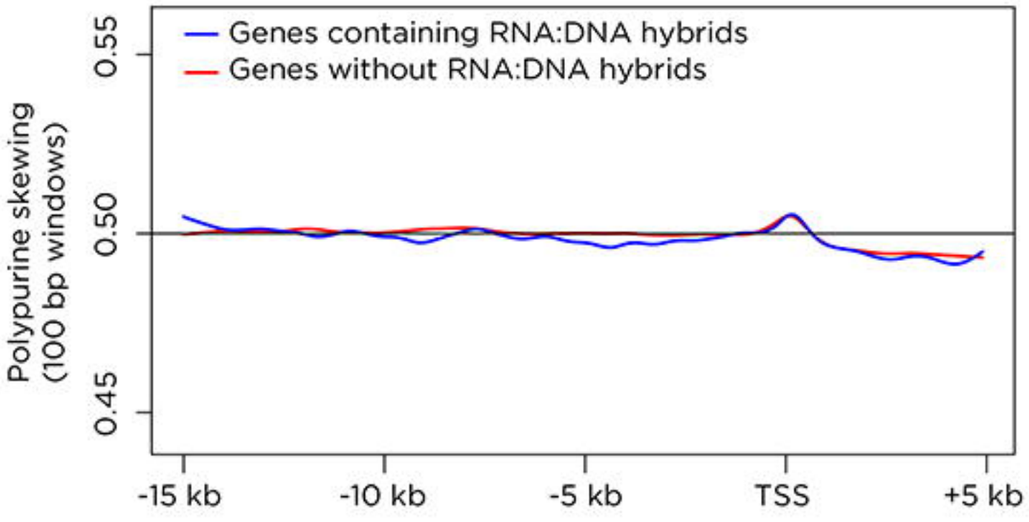

d

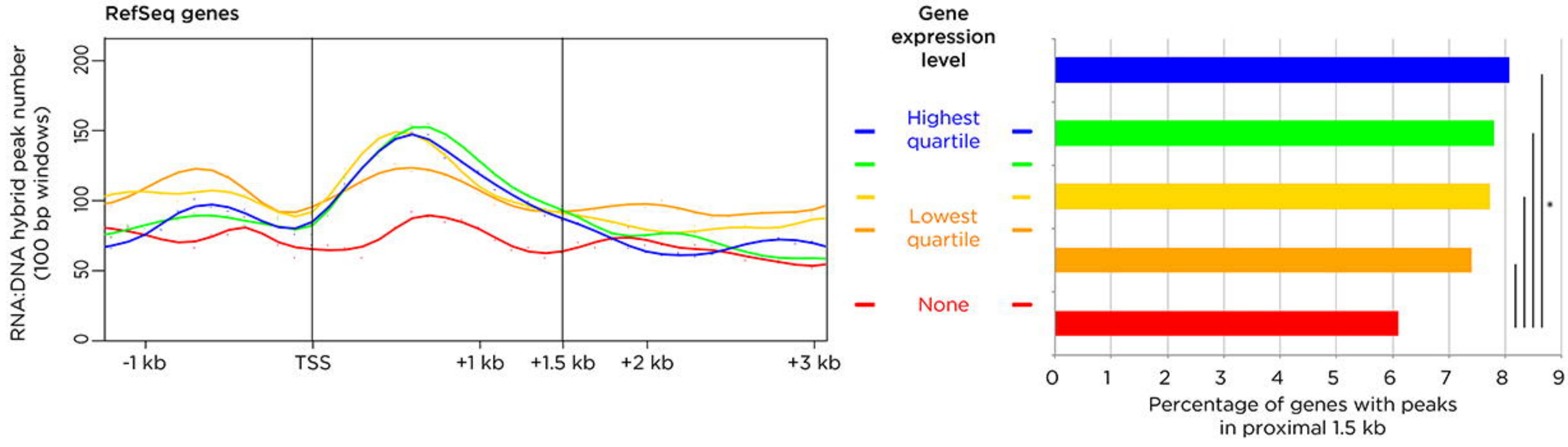

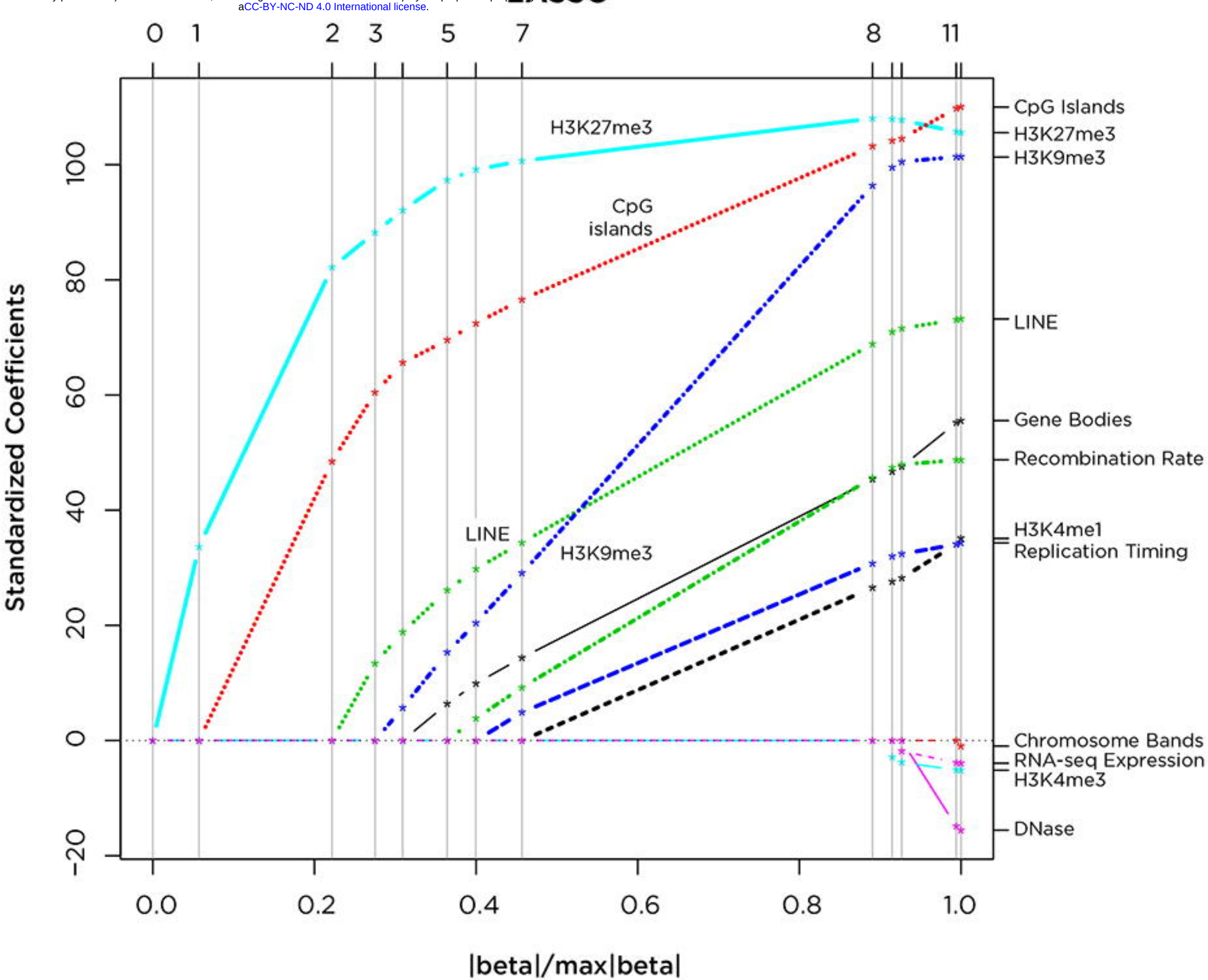

a

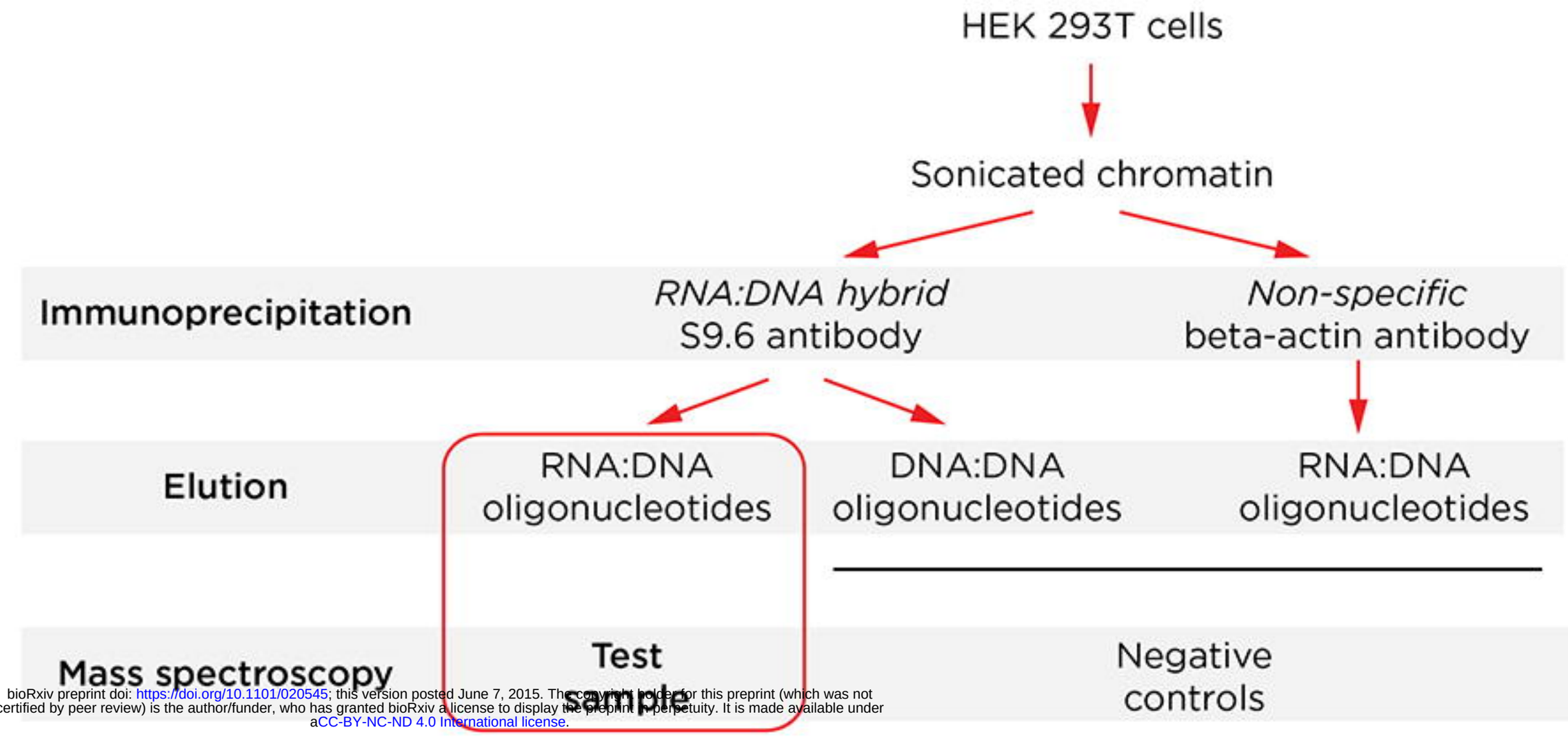

b